UiT
THE ARCTIC UNIVERSITY OF NORWAY

Faculty of Science and Technology

Mechanical and Impact tests of CFRP

An experimental and numerical study of the mechanical properties of CFRP samples with varying temperatures, using Four-point bending, Charpy and Air gun tests

Cathrine Høgmo Strand

Master thesis in Technology and Safety in the High North, June 2017

Project report – Page 2

UiT, The Arctic University of Norway

Department of engineering and safety

9037 TROMSØ

Study program:	**Technology and Safety in the High North**	**Year:**	**2017**

Title: **Mechanical and Impact tests of CFRP** An experimental and numerical study of the mechanical properties of CFRP samples with varying temperatures, using Four-point bending, Charpy and Air gun tests	Date: 1st of June 2017 Classification: Unclassified Number of pages: 61 Attachments: 4
Writer: **Cathrine Høgmo Strand**	
Confidentiality: Open	
Supervisor: **Hassan Abbas Khawaja**	
Contracting authority and assigner: **UiT, The Arctic University of Norway**	

Project description:
This project aims to study the mechanical properties of CFRP with varying temperature settings. The experimental tests being performed is a four-point bending test and two types of impact tests; air gun impact and Charpy impact. Numerical tests are being performed to compare and verify the experimental results.

Cues:
composites, FRP, CFRP, experimental test, numerical test, four-point bending, impact testing, Charpy pendulum test, air gun impact test, numerical analyses, ANSYS Workbench, cold temperatures

Preface

This report is submitted in the course TEK-3901 as a completion of my master's degree in Technology and Safety in the High North at UiT, The Arctic University of Norway.

The work described in this report was carried out at the Department of Engineering and Safety in the spring semester of 2017. It is the original and independent work of author except where specially acknowledged in the text. Neither the present report nor any part thereof has been previously submitted at any other university. This report contains approximately 11500 words, 39 figures and 7 tables.

The experiments are performed at the Safety Lab and the Process Lab at the department. Software used in this report is Microsoft Word, Microsoft Excel, Autodesk Inventor and ANSYS Workbench. It is not assumed that the reader has knowledge to these programs.

It is however assumed that the reader has a general understanding of engineering terms.

Acknowledgements

I would like to acknowledge my supervisor Hassan Abbas Khawaja for the guidance throughout the work of this project, especially the pre-experiment work of constructing the models needed for performing the experiments, and the simulation work in ANSYS Workbench.

I would also like to thank professor Young W. Kwon from the Naval Postgraduate School, California, US, for providing the CFRP samples for this project.

Cathrine H. Strand

Cathrine Høgmo Strand

Abstract

With increasing popularity of carbon fiber reinforced polymer (CFRP) over time, the need of research in the field increases along with it. Many industries demand the benefits of carbon fiber in their installations to be used in harsh environments like cold temperatures, but the research on the temperature exposure behavior of the material is limited. Both strengths and limitations of the applied material should be studied carefully.

Samples of CFRP were provided for this project. The aim of the project was to study the mechanical properties of CFRP with varying temperature settings.

A four-point bending test was performed to find the deflection of CFRP in room temperature, and after being exposed to cold temperature. A numerical test was done to compare and verify the experimental results of the room temperate CFRP.

An air gun impact test was performed to look at the visual effect on the CFRP from a pellet impact and from an ice impact. Permeation was also tested by layering up the CFRP samples to find the limiting thickness for pellet penetration. The results were compared to the results of a numerical analysis.

A Charpy pendulum impact test was used to evaluate the fracture toughness of the CFRP, both qualitative and quantitative.

The results show an overall degradation of mechanical properties of the CFRP samples when exposed to cold temperatures.

Content

Nomenclature

Symbols

b	[mm]	Width of test piece in four-point bending
c	[m]	Perpendicular distance from the neutral axis
d	[mm]	Thickness of test piece in Charpy test
E	[Pa]	Young's Modulus
I	[m^4]	Area moment of inertia
l	[mm]	Length of test piece in four-point bending
L	[mm]	Distance between support points
L_1	[mm]	Distance between support and load points
L_2	[mm]	Distance between load points
L_C	[mm]	Length of test piece in Charpy test
M	[Nm]	Moment
P	[N]	Load
t_{CFRP}	[mm]	Thickness of test piece in four-point bending
x		Reference axis in x-direction
y		Reference axis in y-direction

Greek symbols

δ	Deflection
ε	Strain
θ	Angular deflection
σ	Stress
σ_x	Longitudinal stress

Abbreviations

CFRP	Carbon Fiber Reinforced Polymer
FEM	Finite Element Method
FRP	Fiber Reinforced Polymer
kpm	kilo pound meter
Nm	Newton meter

1 Introduction

A composite is a material that consists of two or more constituent materials or phases that are physically and/or chemically distinct from each other. The characteristics of the composite material are different from the characteristics of any of the components in isolation. [1, 2]

One of the components that is very popular and widely used is fibers like carbon, glass and aramid, and they are reinforced into a fiber reinforced polymer (FRP) composite. [1, 2]

Composites are widely used all over the world throughout different industries, like in the military, the marine and in aerospace. Carbon fiber composites are appreciated for the lightweight, strong and stiff characteristics. The downside of carbon fiber is the expensiveness, but for installations where the characteristics of carbon fiber is highly demanded, the benefits of the material often trumps the costs. [3-5]

After World War II, the military industries interest of FRP's grew rapidly. They started using it for constructing and building boats, which was the beginning of FRP's history in marine applications. [5]

In the marine industry, the stiffness of the carbon fiber is a highly valued factor. Also, the fact that it do not corrode like aluminum and steel make the carbon fiber ideal for marine installations where the material needs to withstand the corrosive marine environment. [5]

The aerospace industry has gained great benefits from the lightweight and strong characteristics of the high-performance carbon fibers in the purpose of saving fuel. The Rutan Model 76 Voyager aircraft managed in 1986 to fly around the world without stopping or refueling. It was the first in the world to achieve such a performance, thanks to the composites used, counting 90% of the structures material. [3, 4, 6]

After this and towards newer times, the use of composites in the aerospace industry has been, and still is rapidly increasing. Carbon fiber composites are used in for example passenger aircrafts, and even for high-temperature applications, such as in the space shuttles because it is relatively temperature resistant. [3, 4]

1.1 Problem overview

With increasing popularity of carbon fiber reinforced polymers (CFRP) over time, the need of research in the field increases along with it. Many industries demand the benefits of carbon fiber in their installations to be used in harsh environments like cold temperatures, but the research on the temperature exposure behavior of the material is limited. Both strengths and limitations of the applied material should be studied carefully.

This project aims to study the mechanical properties of CFRP with varying temperature settings. Numerical tests are being performed to compare and verify the experimental results.

This project and the report is limited to deal with the exact type of CFRP composite provided. The matrix, which functions as a medium for binding and holding the reinforcement together into a solid, is of unknown type in this samples. All other properties are also unknown.

The reinforcing fibers and the matrix (along with the adhesion between the fibers and the matrix) used in each specific type of composite, plays a decisive role for the properties of the reinforced material.

Without knowing the type of matrix used, it is hard to compare, generalize and systemize the results obtained from this project. The results will only be validated for the exact type of CFRP provided for this project, but in general, an overall picture on CFRP characteristics can be drawn from the results, as the tendencies will be the same.

1.2 Thesis outline

This report is divided into seven chapters. The contents of each chapter are described as follows;

- Chapter 2 presents theory and literature review. It is explained what composites are, the history of composites and earlier studies of composites. Some basic mechanical theory is presented. Finally, theory and literature review relevant for the types of tests to be performed in this project is given.

- Chapter 3 presents the methodology of this project. The methodology is presented in different subchapters for each of the three types of test performed; the four-point bending test, the air gun impact test and the Charpy impact test. For the four-point bending test and the air gun impact test, there is also undersections which represents the experimental test and the numerical analyses. For the Charpy test, only experimental test is being presented.

- Chapter 4 presents the results and discussion. The results are presented in different subchapters in the same way as for the methodology.

- Chapter 5 gives a summary of the results and the conclusions.

- Chapter 6 describes the challenges encountered in the work of this project.

- Chapter 7 describes the possible future work with basis in this report.

In addition, a list of references is provided at the end of the report. The related material that wasn't expedient to present in the report is provided as appendixes.

1.3 Clarifications

In this report the reader will find the words sample and test pieces often used. A clarification of the use of these two words in the work of the writer is given:

- **Sample** refers to the CFRP samples provided for this project, just the way they were out of the box, in its entirety.

- In the numerical analyses the word sample is also used to describe the body which is assigned with CFRP as material (in ANSYS Workbench) to refer to the samples provided for this project.

- **Test piece** refers to the pieces custom cut from the samples to fit each test.

2 Theory and literature review

In this chapter the theory and literature review relevant for this project is presented. It is explained what composites are, the history of composites and earlier studies of composites. Some basic mechanical theory is presented. Also, theory and literature review relevant for the types of tests to be performed in this project is given.

2.1 Composites

A composite material consists of two or more constituent materials or phases that are physically and/or chemically distinct from each other. The characteristics of the composite material are different from the characteristics of any of the components in isolation. [1, 2, 7, 8]

The two composite components relevant for this report are reinforcing fibers and matrix. The fibers are the discontinuous or dispersed phase and the matrix acts as the continuous phase. In addition, there will also be an interphase or interphase region, but this part will not be covered in this report. [7]

The matrix is a homogeneous and monolithic material which functions as a medium for binding and holding reinforcements together into a solid. In addition, it will provide finish, texture, color, durability and functionality as well as protecting the reinforcements from environmental damage. [7]

The reinforcing fibers and the matrix used in the specific type of composite, plays a decisive role for the properties of the reinforced material. The final mechanical properties will also be dependent on the adhesion between the fibers and the matrix because the stress transfer between matrix and fibers determines the reinforcement efficiency. [7, 9]

The fibers used for reinforcement are carbon, glass and aramid. Fiber reinforced polymer composites (FRP) are subdivided into [7, 9]:

- Carbon fiber reinforced polymer composites (CFRPs)
- Glass fiber reinforced polymer composites (GFRPs)
- Aramid fiber reinforced polymer composites (AFRPs)

Matrix is subdivided into [7, 9]:

- Polymer matrix
- Metal matrix
- Ceramic matrix

As FRP's are polymer composites, the matrix used is polymer matrix. One of the most used polymer matrixes is resin.

2.1.1 History of composites

Composite materials are originally an idea of nature. An example of that is wood, which is a fibrous composite built up by cellulose fibers in a lignin matrix. The cellulose fibers have low stiffness and high flexibility, but the lignin matrix united with the fibers provide stiffness which makes it a reinforced composite. Another example of a composite created by nature is bone. Short and soft collagen fibers embedded in a mineral matrix called apatite makes the bone able to support the weight of for example the human body. [2, 10]

The history of human made composites probably has its origin from around year 3400 BC when the Mesopotamians glued wood strips at different angles to create plywood. Later on, the ancient Egyptians used cartonnage, layers of linen or papyrus soaked in plaster, to mask dead people, known as mummification. Around year 1500 BC, the Egyptians also started using clay reinforced with reeds to create bricks as building material for houses. This method is still well known today. [1, 10-12]

Throughout history, composites have played an important role to humans. The strive have always been to make better, stronger and more lightweight composite materials. The development of different fiber materials and the improvements of filler materials (resins) to be used has made FRP a growing industry. [9, 10]

In the late 1800s a synthetic resin was made that could transform from liquid state to solid state by crosslinking molecules. This process is called polymerization, from which the name polymer resins were given. [11, 12]

In the 1930s other high-performance resin systems, including unsaturated polyester resins and epoxy resins became available. Glass fiber, made by drawing glass into thin fibers and weaving it into a textile fabric, combined with this newer synthetic polyester resins, produced strong and lightweight composites that made for a new era in for example the boating industry. [9, 11, 12]

The first carbon fiber was patented in 1961, but it took several more years for carbon fiber composites to be used commercially. At the same time aramid fibers were being produced. [11, 12]

In the mid-1990s, mainstream manufacturing and construction of composites made for new opportunities, and composites became more generally known and more widely used. [11, 12]

Today, FRP is used widely in industry for any applications that require plastics with specific strength or elastic qualities. Glass fibers are the most common across all industries, although carbon-fiber and carbon-fiber-aramid composites are widely found in for example aerospace, automotive, marine and sporting good applications. [3-5, 11, 12]

2.2 Composites in cold climate

Most materials are affected somehow by environmental effects such as temperature and humidity, etc. The properties and characteristics may change and the material can be weakened or damaged. [8]

A harsh environment can have profound effects on the polymer-based composites, including most CFRPs. The right combination of moisture and temperature can affect the carbon fibers or the matrix, as is the situation in most cases, and lead to degradation of the mechanical properties of the CFRP. [8]

It is reasonable to assume that the strength of composites will decrease when exposed to cold temperatures. Research have been done, showing several outcomes. For example, Bulmanis et. al [13], Alan T. Nettles and Amily J. Biss [6] and Shang-Lin Gao and Jang-Kyo Kim [14].

Kasen [15] studied the behavior of composites at very low temperatures (cryogenic) and observed that it is hard to obtain a systematic data base for composites at lower temperatures. Existing data show extreme variability in strength properties, probably because different matrixes/resins provides different properties to the composite. [8, 15]

CFRP is a complex material, and the properties are very dependent on the layup process and the specific type of matrix/resin used. It is therefore hard to establish “rules” of properties and characteristics that will apply to all CFRP. [8]

2.3 Basic mechanical theory

To understand some of the basic mechanical theory behind the properties of a material, it is first important to be able to distinguish different expressions from one another [16]:

- **Stiffness** of a material is a measure of the amount of force needed to deform or permanently change its original shape.
- **Strength** of a material is a measure of the amount of force it can withstand and still recover its original shape.
- **Hardness** of a material defines the relative resistance that its surface imposes against the penetration of a harder body.
- **Toughness** is a measure of the amount of energy that a material can absorb before fracturing.
- **Strain** is a measure of proportional deformation (amount of bend or stretch) in a material.
- **Stress** is a measure of force per unit area applied to the material.

Elastic deformation is when a material returns to its original shape after an applied load is being removed. In the range where the ratio between load and deformation remains constant, the stress-strain curve is linear. [16]

Plastic deformation is an irreversible deformation to a material. To reach to plastic deformation the material will first go through elastic deformation. [16]

A general stress/strain curve is shown in figure 1, where the elastic and the plastic region can be seen. The material will undergo elastic deformation until it reaches the yield point and plastic deformation starts. When the material has been exposed to a stress equal to the ultimate strength of the material, the material will eventually fracture if the exposure to stress continues.

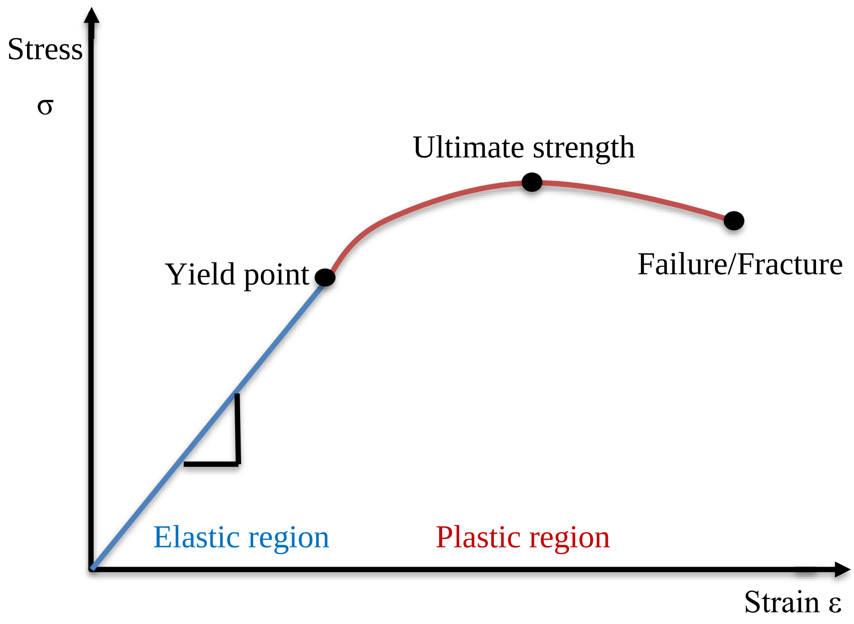

Figure 1 – A general stress/strain curve

2.3.1 Young's modulus / modulus of elasticity

Young's modulus, also known as the elastic modulus, is a measure of the stiffness of a solid material. Higher stiffness of the material gives a higher Young's modulus. It tells us how much a material bends/strains under a given load/stress. [16]

Young's modulus is expressed as a ratio of stress to strain. Its SI unit is Pa (N/m^2), but the more practical way to express the unit would be GPa (kN/mm^2 or 10^9 N/m^2).

$$Young's\ Modulus, E\ = \frac{Stress}{Strain}\ \ [Pa]$$ [6]

For most materials, the Young's modulus will increase when the temperature decreases. [8]

2.3.2 Tensile strength and compressive strength

Tensile strength is the ability of a material to withstand a tensile (pulling) force tending to stretch the material. In other words, tensile strength resists tension (being pulled apart). Ultimate tensile strength is measured by the maximum stress that a material can withstand while being stretched or pulled before failure, such as breaking or permanent deformation. [17]

The opposite of tensile strength is the compressive strength, which is the capacity of a material to withstand a compression (pushing) force tending to reduce the size of the material. In other words, compressive strength resists compression (being pushed together). The ultimate compressive strength is measured by the value of uniaxial compressive stress the material has reached when it fails completely. [17]

Composite materials, such as CFRP tend to have higher tensile strengths than compressive strengths.

As strength is measured by applied stress, the units are force per unit area.

2.1 Four-point bending

Four-point bending is based on the Euler-Bernoulli beam theory. A four-point bending test provides different values to obtain the properties of a material. The four-point bending test is similar to the three-point bending test. A load is applied in the center of the length of a beam, but with the addition of a 4th bearing which spreads the maximum stress over a larger portion of the beam. A schematic of the four-point bending test setup is shown in figure 2. The beam is placed on top of two support bearings (support points) (a), and on top of the beam there are two centralized loading bearings (load points) (b) with equal distance from the supports. [18]

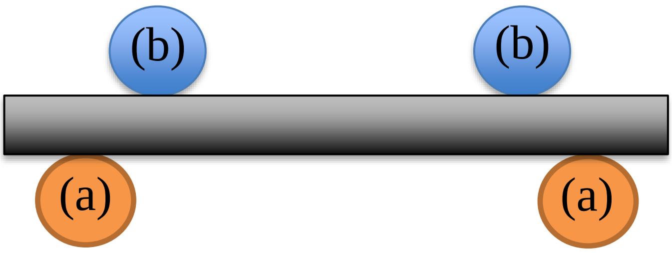

Figure 2 – A schematic of a four-point bending test setup

2.2 Impact testing

Impact energy is a measure of the work done to fracture a material. In other words, it is a measurement on how much energy a material will absorb before failure occurs. In this project, two types of impact tests will be considered. The first is an air gun impact test, where a pellet is shot at high speed onto the test samples to get a visual display of the occurring failure modes of the CFRP and to test the permeability. The air gun impact test is qualitative.

The Charpy impact test on the other hand, will provide quantitative results in addition to the qualitative, telling us how much energy the CFRP samples can absorb before failure occurs.

2.2.1 Charpy impact test

The Charpy impact test is a standard low-velocity and high-strain pendulum impact test used for evaluating fracture toughness. A specimen is stroke with a controlled weight pendulum swung from a set height as seen in figure 3. [19-21]

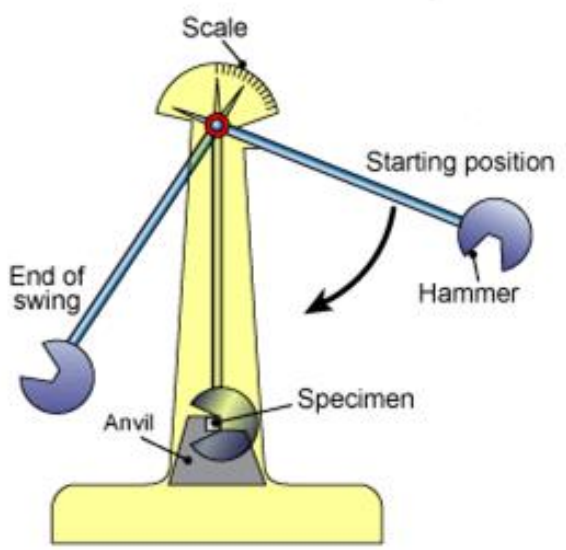

Figure 3 – A schematic of the Charpy pendulum [19]

The test determines the amount of energy a material can absorb before fracture and failure occurs. [19-21]

The Charpy test is easy to set up. The test is very easily and quickly performed, and results will be obtained right away. This, in addition to the Charpy pendulum device being cheap and moveable, makes it a widely applied testing mechanism in industry and for research on materials. In general, pendulum impact tests are subject to errors due to kinetic energy and vibrational losses, but these losses are so small that they are negligible. [20, 21]

The test piece with its geometric variables will play an important role on the values being measured. One of the geometric variable is the span-to-thickness ratio (L_C/d), as seen in figure 4.

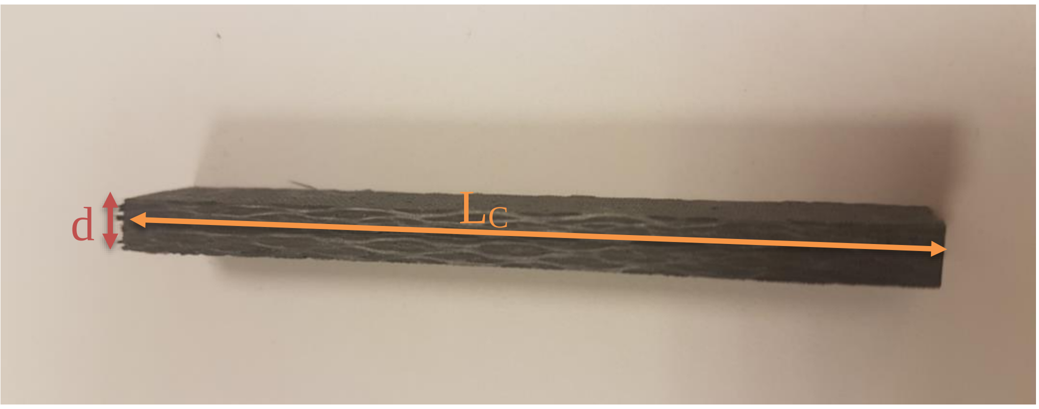

Figure 4 – The span-to-thickness ratio (L_C/d) of a test piece of CFRP.

Bader and Ellis [20] studied the effect of different span-to-thickness ratios in the measuring of impact strength in unidirectional composites and found that the dominating failure mode with a span-to-thickness ratio (L_C/d) less than 10 is delamination. The recorded impact strength was assumed to be artificially high in this case. They also suggested that $L_C/d \geq 10$ would give more trustworthy results. This can be seen in figure 5. [20, 21]

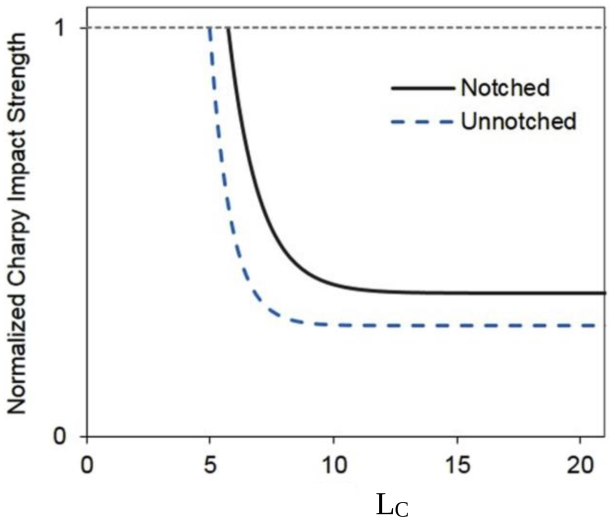

Figure 5 – Generalized relationship between Charpy impact strength and geometry (L_C/d) for test pieces with and without notches. [20]

It should be noted that the Charpy test can be run on both notched and unnotched test pieces as seen on figure 6, depending on material. For FRP, both types can be used. [20, 21]

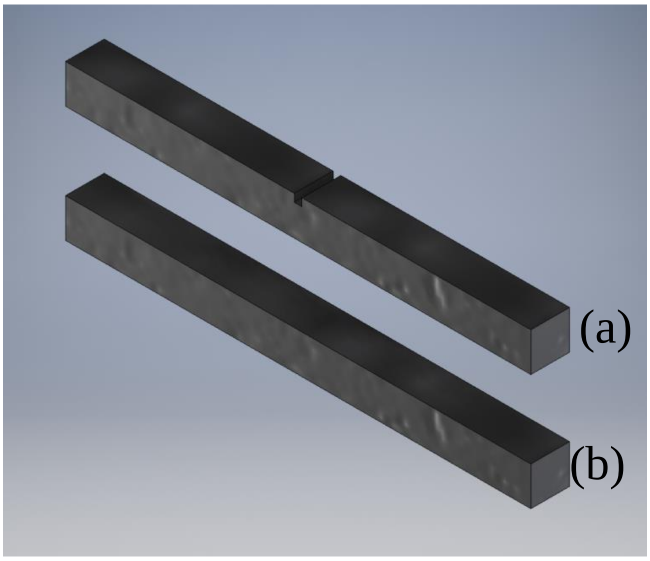

Figure 6 – A display of a notched CFRP sample (a), and a unnotched CFRP sample (b).

The results obtained from Charpy tests could be evaluated quantitatively or qualitatively. The one thing in common for quantitatively and qualitatively results is that they in most cases should be used as comparative results only.

Quantitatively:

The quantitative results obtained from the test will be the amount of energy needed to fracture the material given by the force performed by the pendulum given in kpm.

Qualitatively:

The qualitative results obtained from the test is more of a visual result and can be used to determine the type of failure mode occurred to the material in the fracture.

The failure modes for CFRP can essentially be divided into two general categories:

(i) fiber-dominated failure (cut off)
(ii) matrix-dominated failure (delamination)

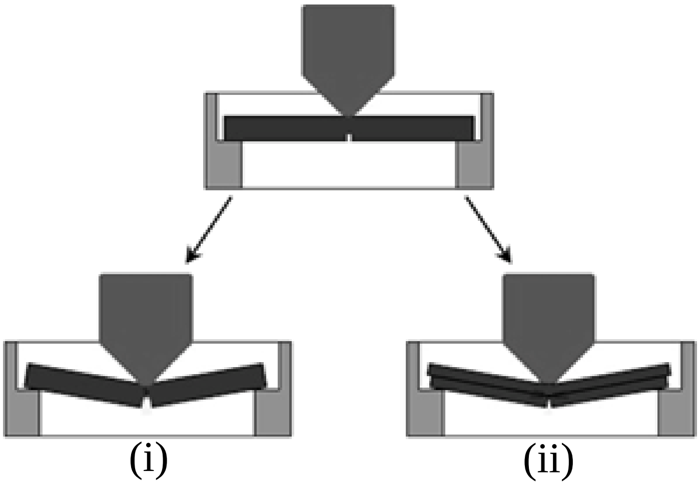

Figure 7 – The dynamic fracture process in CFRP during Charpy impact testing after the instant of striker impact. The impact can lead to fiber dominated failure (i) which is seen as a cut off of the test piece, and matrix-dominated failure (ii) which can be seen as delamination in the test piece. [21]

Normally a material will not break in only one way or the other, but by comparing the amount of different failures in a representative selection of samples of the same material, an estimate of the most common fracture, hence the failure mode can be given.

2.3 Finite Element Method

Partial differential equations are commonly used to describe the laws of physics for space and time dependent problems. These equations are often not solvable with analytical methods, and an approximation of the equations is needed, typically based upon different types of discretizations. These discretization methods approximate the partial differential equations with numerical model equations, which can be solved using numerical methods. This means that the solution to the numerical model equations approximate the real solution to the partial differential equations. [22]

One of the methods used to compute such approximations is the finite element method (FEM). The method is commonly used to solve problems of engineering and mathematical physics. [22]

When using the finite element method, a finite element mesh is created, and the accuracy that can be obtained from any model is directly related to mesh density. The mesh subdivides the model into smaller domains called elements, over which a set of equations are solved. As the mesh is refined with smaller and smaller elements, the computed solution will converge against the realistic solution. [22]

3 Methodology

The methodology is presented in different subchapters for each of the three types of test performed; the four-point bending test, the air gun impact test and the Charpy impact test. For the four-point bending test and the air gun impact test, there are also undersections which represents the experimental test and the numerical analyses. For the Charpy test, only experimental test was performed.

All the experimental tests described under this chapter has been done in the Safety Lab and the Process Lab at UiT, The Arctic University of Norway, spring 2017. The cold room in the Safety Lab has been used for exposure of the CFRP samples to cold temperature. It should be noted that the temperature in the cold room is not consistent. It is regulated externally, and not by the students. Opening/closing of the door will also affect the temperature on a short term. However, it is assumed that the temperature is kept in a range between -10˚C and -30˚C. Whenever it was possible to take reading of a valid temperature during experiments, the temperature is presented in the methodology. The numerical analyses have been performed on a Lenovo P910 computer.

3.1 CFRP test samples

All the test samples used in this project are of the brand DragonPlate, manufactured by Allred and Associates Inc., an engineering product development and manufacturing firm in business since 1993, located in Elbridge, New York. [23]

The two types of DragonPlate CFRP samples provided for this project are:

- 6 pieces of:
  EconomyPlate™ Solid Carbon Fiber Sheet ~ 1/32" x 12" x 12"
  → The sizing converts to 0.79375 mm x 304.8 mm x 304.8 mm in SI-units.
  This pieces will in this report be referred to as the thin samples.

- 2 pieces of:
  EconomyPlate™ Solid Carbon Fiber Sheet ~ 5mm x 12" x 12"
  → The sizing converts to 5 mm x 304.8 mm x 304.8 mm in SI-units.
  This pieces will in this report be referred to as the thick samples.

The company has this product description on their web pages:

“For less demanding applications where you can live without the optimized material properties of a quasi-isotropic layup, we have created EconomyPlate. Our EconomyPlate™ sheets are comprised of orthotropic (non-quasi-isotropic) laminates utilizing a twill weave at 0°/90° orientation, while maintaining a symmetrical and balanced laminate. For this sheet size, we offer twill high gloss, matte or textured finish on one side and a textured finish on the other side providing an excellent bonding surface. As with all DragonPlate solid carbon fiber sheets, EconomyPlate™ is composed entirely of a tough and rigid carbon reinforced epoxy matrix.” [24]

The difference in a quasi-isotropic layup and a non-quasi-isotropic layup lies in the way the sheets are placed on top of each other in the layup process. In a quasi-isotropic layup, an additional sheet in the 45-degree diagonal direction is placed between the 0/90 sheets to strengthen the laminates in this direction. An illustration of this, made by the manufacturer of the samples can be seen in figure 8. [25]

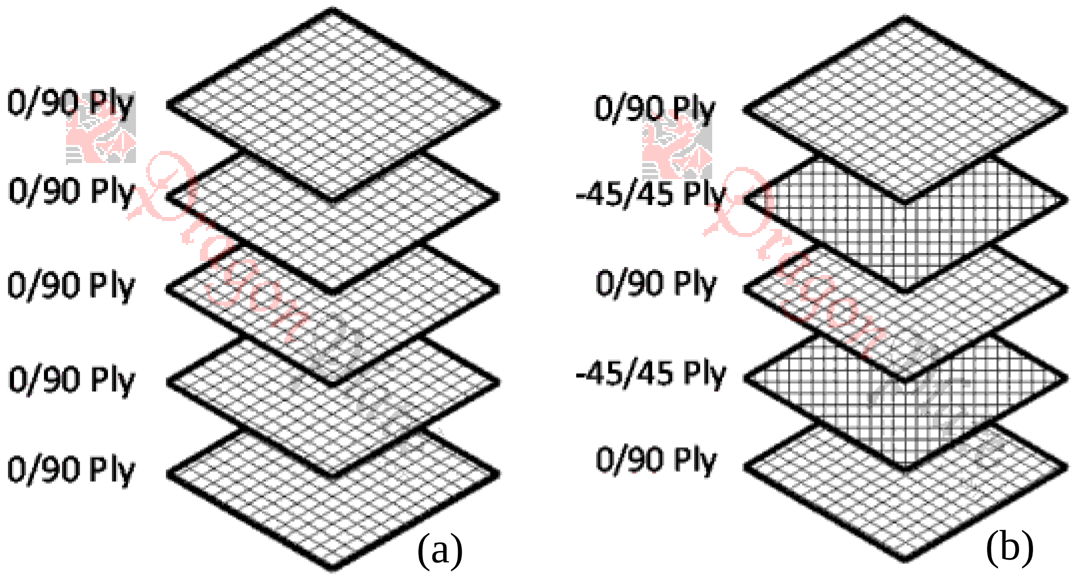

Figure 8 – An illustration of the difference between a non-quasi isotropic layup (a) and a quasi-isotropic layup (b). [25]

The non-quasi isotropic samples will have the same strength in both length/width directions, but will lack some strength in the diagonal direction. This is however dependent on the layup process. In this project, all the tests were performed over the lengths of the samples and not in the diagonal direction.

It should be noted that not only the strength, but also properties such as Young's Modulus, change with direction along the sample. Therefore, CFRP is considered an anisotropic material. [8, 17]

3.2 Four-point bending

3.2.1 Experimental test

To perform the test, a device had to be built from scratch. The device to be built were first planned by dimensioning it with reasonable values to fit the test pieces. The parameters of both the test device and the test pieces is seen in table 1.

Table 1 – The parameters of the four-point bending test device and the test pieces

Description	Variable	Value (mm)
Length of test piece	l	304.8
Width of test piece	b	60
Thickness of test piece	t_{CFRP}	5
Distance between support and load points	L_1	20
Distance between load points	L_2	160
Distance between support points	L	200

With the dimensions ready, the device was modelled in Autodesk Inventor. The model can be seen in figure 9. It consists of a movable upper frame with the load points on (a), and a lower frame which is standing on a plane surface and have the support points mounted on to it (b). The CFRP test piece (c) is placed on top of the support points.

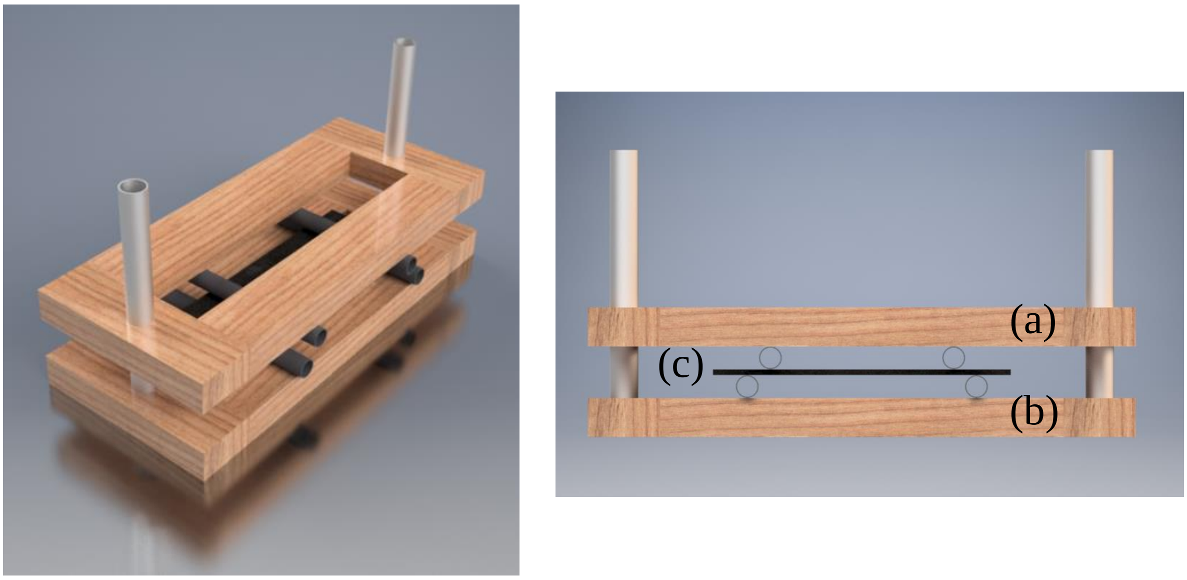

Figure 9 – The test device for four-point bending tests, modelled and dimensioned.

The finished hand-made device is seen in figure 10.

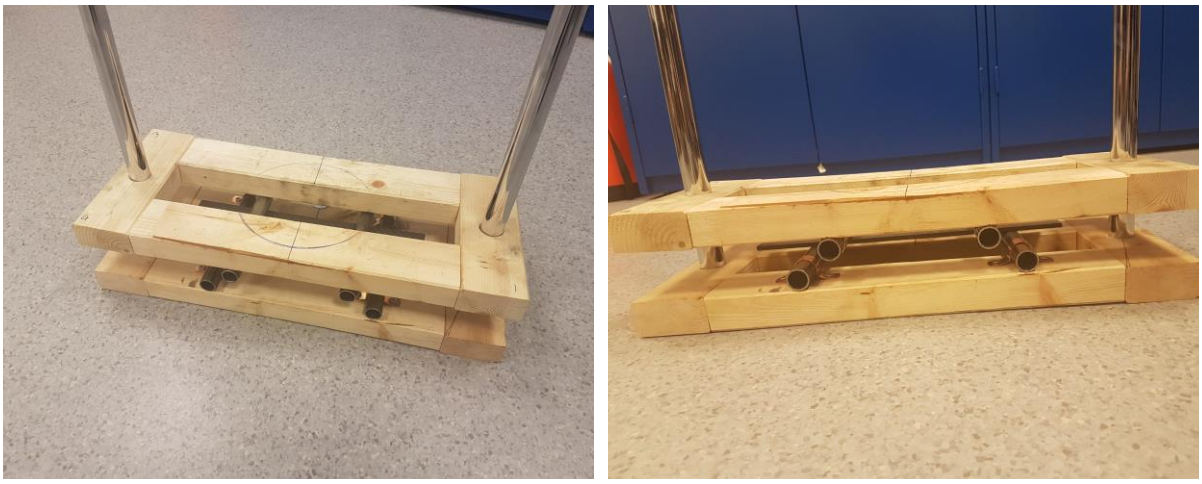

Figure 10 – The test device for four-point bending tests, built by hand.

The test was performed by placing the test piece on the support points of the lower frame, and then the upper frame was slid down with the load points resting on the test piece.

Measurements were taken between the lower point of the upper frame and the upper point of the lower frame on all four corners to ensure that a possible tilt of the upper frame would not affect the results. The four values are being averaged for further use.

The measurements should account for an error of +/- 0,005 mm due to measuring equipment sensitivity.

The measurements were taken before any additional weight was applied on top of the upper frame and then after the weight was applied onto the center point of the upper frame. A weight of 15 kg was used. The upper frame weights 1,3 kg, giving a total of 16,3 kg.

The difference between the measurements taken before and after applied weight gives the deflection of the beam at load points.

The measurement of deflection was done on CFRP test pieces of room temperature, and on test pieces that had been exposed to cold temperature in the cold room for a week.

Four-point bending is based on the Euler-Bernoulli beam theory, and the equation for bending moment in a beam is given [26]:

$$\frac{d^2y}{dx^2} = \frac{M}{EI} \tag{3.1}$$

When the angle of deflection is very small, $tan\theta = \frac{dy}{dx}$ can be written as $\theta = \frac{dy}{dx}$. Therefore, equation (3.1) can be rewritten to equation (3.2):

$$\theta = \int \frac{M}{EI} dx \tag{3.2}$$

From equation (3.2), the equation for displacement y, equation (3.3) can be derived:

$$y = \int \theta \, dx = \iint \frac{M}{EI} dx \tag{3.3}$$

Where M is moment, E is Young’s Modulus and I is the area moment of inertia.

When a total force is applied to the two load points at equal distance from the two support points, it results in shear force and a bending moment which are shown in figure 11.

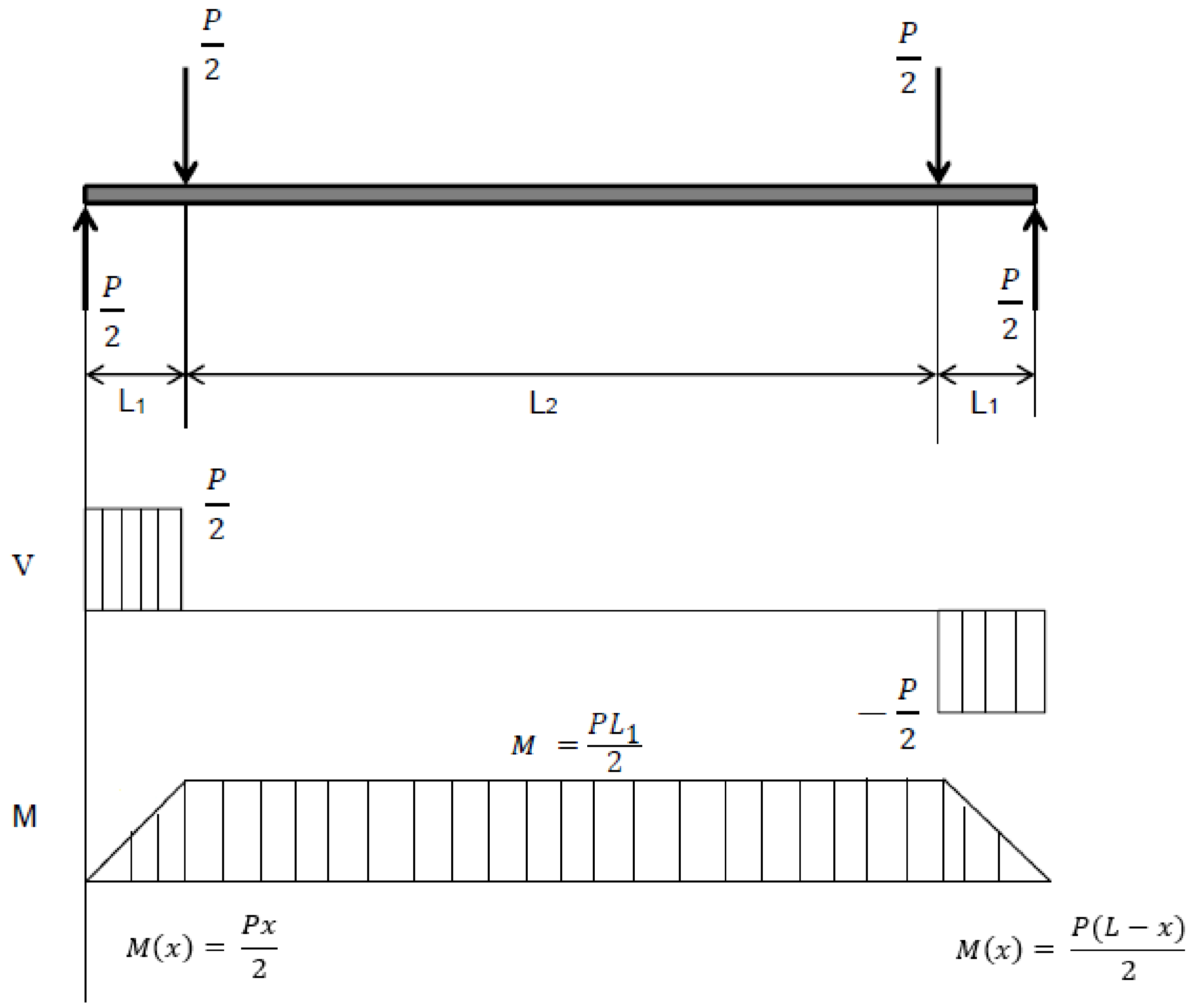

Figure 11 – The four-point bending set-up with the shear force diagram (V) and the bending moment diagram (M).

- P is the total load, given in N
- L_1 is the distance between the support points, given in mm
- L_2 is the distance between load points, given in mm
- $L = L_1 + L_2$, which is the total length of the beam, given in mm
- M is the moment, given in Nm
- x is the distance from the load point to the nearest support point, given in mm

The moment in the middle of the beam is constant, however it is a function of x at both ends as shown in equations (3.4):

$$M(x) = \frac{Px}{2} \qquad 0 \le x \le L_1$$

$$M = \frac{PL_1}{2} \qquad L_1 \le x \le (L_1 + L_2) \tag{3.4}$$

$$M(x) = \frac{P(L-x)}{2} \qquad (L_1 + L_2) \le x \le L$$

The angle θ and the deflection δ for the three moment regions of the beam are given in equation (3.5) to (3.10):

For $0 \le x \le L_1$ and $M = \frac{Px}{2}$:

$$\theta_1 = \frac{Px^2}{4EI} + C_1 \tag{3.5}$$

$$\delta_1 = \frac{Px^3}{12EI}\theta_1 + C_1 x + C_3 \tag{3.6}$$

For $L_1 \le x \le (L_1 + L_2)$ and $M = \frac{PL_1}{2}$:

$$\theta_2 = \frac{PL_1 x}{2EI} + C_2 \tag{3.7}$$

$$\delta_2 = \frac{PL_1 x^2}{4EI} C_2 x + C_4 \tag{3.8}$$

For $(L_1 + L_2) \le x \le L$ and $M = \frac{P(L-x)}{2}$:

$$\theta_3 = -\frac{Px^2}{4EI} + \frac{PLx}{2EI} + C_5 \tag{3.9}$$

$$\delta_3 = -\frac{Px^3}{12EI} + \frac{PLx^2}{4EI} + C_5x + C_6 \tag{3.10}$$

The six equations $\theta_1, \theta_2, \theta_3, \delta_1, \delta_2$ and δ_3 have six unknowns; C_1, C_2, C_3, C_4, C_5 and C_6. To solve the equations, six boundary conditions are needed, as seen in equations (3.11) to (3.15):

$$x = 0, \qquad \delta_1 = 0, \tag{3.11}$$

$$x = L_1, \qquad \delta_1 = \delta_2, \qquad \theta_1 = \theta_2 \tag{3.12}$$

$$x = \frac{L}{2}, \qquad \theta_2 = 0 \tag{3.13}$$

$$x = L - L_1, \qquad \delta_2 = \delta_3, \qquad \theta_2 = \theta_3 \tag{3.14}$$

$$x = L \qquad \delta_3 = 0 \tag{3.15}$$

Solving the equations with the boundary conditions gives equations (3.16) to (3.21):

For $0 \leq x \leq L_1$:

$$\theta_1 = \frac{P}{4EI}(L_1L - L_1^2 - x^2) \tag{3.16}$$

$$\delta_1 = \frac{Px}{12EI}(3L_1L - L_1^2x - x^2) \tag{3.17}$$

For $L_1 \leq x \leq (L_1 + L_2)$:

$$\theta_2 = \frac{PL_1}{4EI}(L - 2x) \tag{3.18}$$

$$\delta_2 = \frac{PL_1}{12EI}(3Lx - L_1^2 - 3x^2) \tag{3.19}$$

For $(L_1 + L_2) \leq x \leq L$:

$$\theta_3 = -\frac{P}{4EI}(x^2 + L_1^2 + L^2 - LL_1) + \frac{PLx}{2EI} \tag{3.20}$$

$$\delta_3 = -\frac{P}{12EI}(x^3 - L^3) + \frac{P}{4EI}(Lx^2 - L_1^2x - L^2x + LL_1x + L_1^2L - L^2L_1) \tag{3.21}$$

Because CFRP is an anisotropic material, the Young's Modulus, E will change with changing deflection of the beam. The Young's Modulus of tension under the beam, and the Young's Modulus of compression at the top of the beam may also be different from each other.

However, the longitudinal stress in the beam is directly proportional to the applied load and does not depend on the Young's Modulus. The Euler-Bernoulli beam theory states that stresses vary linearly with the distance from the neutral axis:

$$\sigma_x = \frac{M|c|}{I} \tag{3.22}$$

Where σ_x is the longitudinal stress in Pa, M is the moment about the neutral axis in Nm, c is the perpendicular distance from the neutral axis in m and I is the area moment of inertia about the neutral axis in m^4.

If an applied load causes more stress than the tensile strength of the material it will fracture. The maximum stress is therefore limited by tensile strength.

3.2.2 Numerical analysis

The numerical analyses were performed in ANSYS Workbench. The geometric model is seen in figure 12.

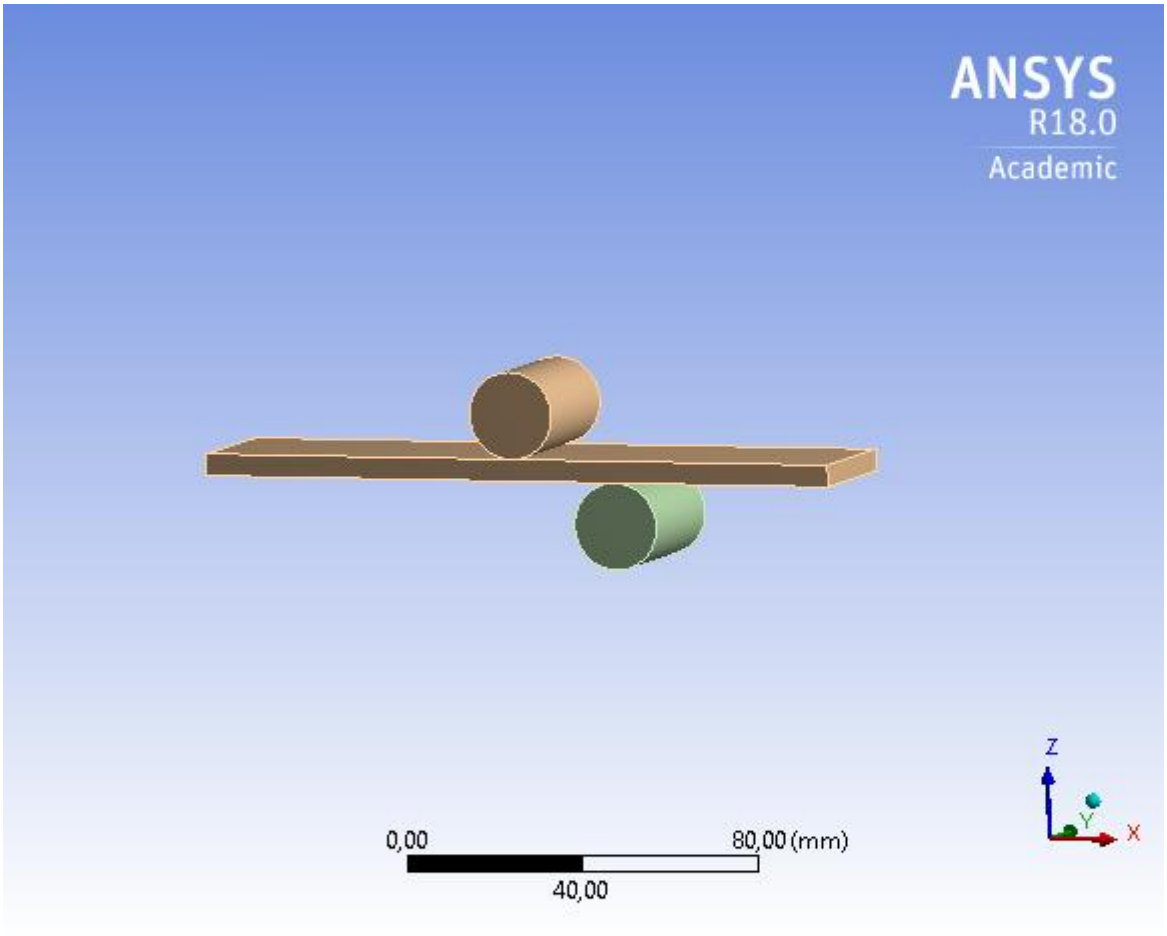

Figure 12 – The geometric model for the four-point bending numerical analysis in ANSYS Workbench

Symmetry was used on the model in both y-direction and negative x-direction (as seen in the figure) to ease the computational load of the simulation. The dimensions of the CFRP test piece, the support and the load points are the same as in the experimental test as seen in table 1, chapter 3.2.1.

To create a finite element (FE) model, an automated mesh was generated in ANSYS Workbench. The meshing of the model was limited by the number of elements/nodes allowed in the Academic license of ANSYS Structural physics, which is 32 000 nodes/elements. A mesh sensitivity analysis was performed by increasing the number of nodes and elements to see when the solution to the simulation converged. The highlighted mesh parameters are seen in table 2, for full list see Appendix A.

Table 2 – The mesh parameters for the FE model for the four-point bending analysis in ANSYS Workbench

Physics preference	Mechanical
Relevance	-95
Element Midside Nodes	Dropped
Relevance Center	Fine
Element size	1,50 mm
Span Angle Center	Coarse
Nodes	**29031**
Elements	**24750**

The material assigned to the CFRP sample was the Epoxy Carbon Woven (230 GPa) Wet, with pre-defined parameters in ANSYS. It should be noted that the CFRP material used for simulations is assumed quasi-isotropic, which is not the real case of the CFRP samples in this project. The material assigned to the support and load points (the cylinders) was structural steel, with pre-defined parameters in ANSYS. The parameters of both materials are shown in Appendix A.

A cylindrical support was placed on the support cylinders to ensure they are not moving. A displacement in the negative z-direction was placed on the load cylinders.

The results of this analysis are presented and discussed in chapter 4.1.2.

3.3 Air gun impact

3.3.1 Experimental test

An air gun impact test was performed to provide visual results of the failure mode created by the impact of the pellet hitting the CFRP samples at high speed. The thin samples were used for this test. The rate of permeation in the material were also tested by creating a buildup of several layers of the thin samples.

The test was performed in room temperature on tempered test pieces at about 22˚C and in the cold room on test pieces exposed to about -28˚C for 7 days.

To the purpose of performing the impact tests with the air gun, a shooting box were built, seen in figure 13. This allows for safety under the shooting, as the box gathers up the pellets that passes through the test pieces. The box consists of an opening-closing system with locking screws and wingnuts, so test pieces could be fastened for testing, and removed and replaced with new test pieces effectively. This is shown in figure 14.

Figure 13 – The shooting box

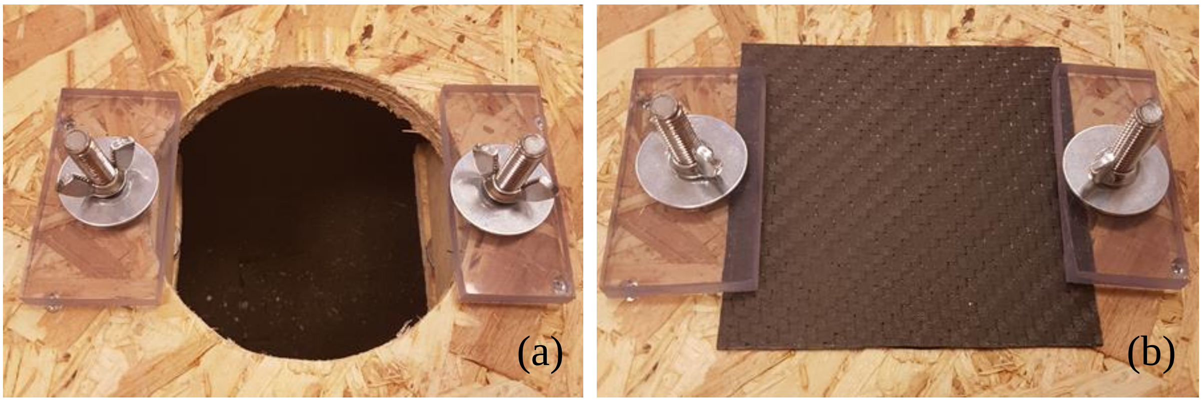

Figure 14 – The opening-closing system of the shooting box, seen without a test piece (a) and with a test piece fastened (b).

The air gun used for the tests is a standard shotgun type. A ruler was placed on the barrel of the gun to measure the shooting distance.

Figure 15 – The air gun used in this project

Figure 16 – To shoot at exact 60 mm distance from the test pieces, a ruler was attached to the barrel of the gun.

Two different pellets were chosen for this test to see if they would make different failures to the CFRP. The material of both pellets is lead and they are of 4,5 mm caliber, weighing about 0,5 grams each.

Both pellets can be seen in figure 17. The standard Diabolo pellet (a) has a flat tip and the Storm pellet (b) has a soft pointed tip.

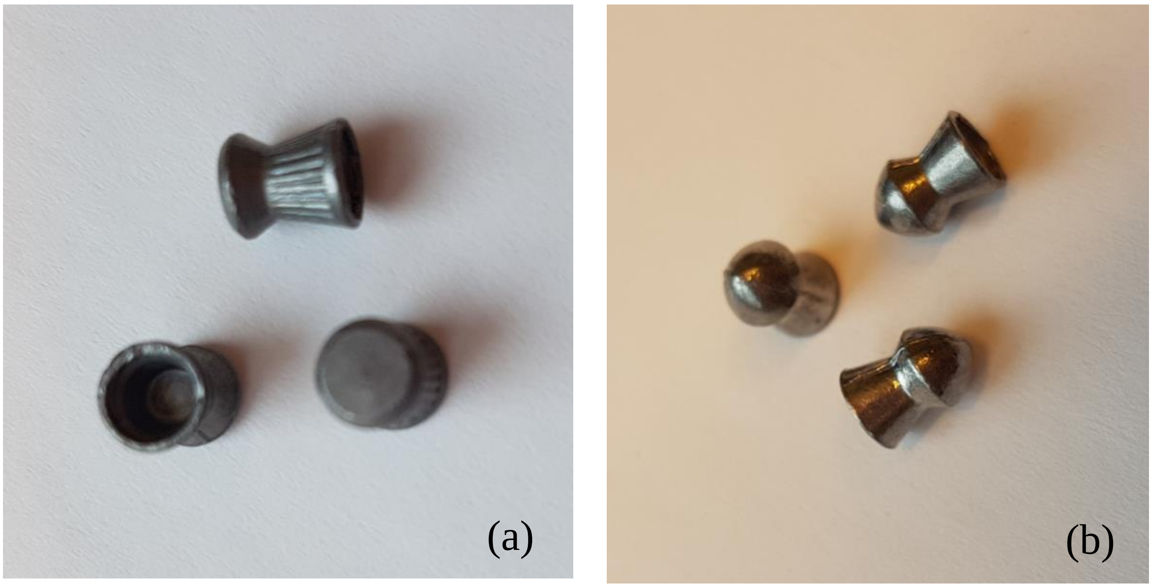

Figure 17 – The standard Diabolo pellet (a) and the Storm pellet (b).

A speed test was carried out using a high-speed camera. The Diabolo pellet was fired with a scale in the background. The test showed a pellet speed of 160 m/s. (Appendix C)

For this experiment the thin CFRP samples were cut into 100x100 mm test pieces to fit the hole on the shooting box. For the visual impact failure mode test, single layered test pieces were used. For the permeation test, a built up of 1-4 layers was made like shown in figure 18.

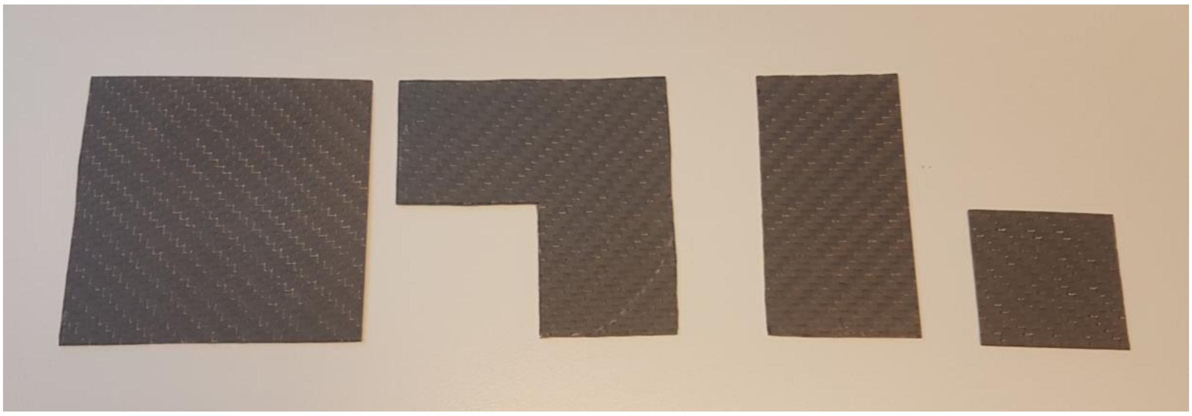

Figure 18 – A built up of 1-4 layers of CFRP test pieces is obtained by sliding all the pieces to the left on top of the square piece.

The test setup for the shooting was to manually fire off the gun, vertically towards the test piece fastened in the shooting box placed on steady ground. The shooting distance was of 60 mm.

3.3.2 Numerical analysis

The numerical analyses were performed in ANSYS Workbench. The geometric model of the Diabolo pellet was created in Autodesk Inventor and imported to the ANSYS Workbench Explicit Dynamics module where the CFRP sample was created. The pellet was then aligned at the shooting range of 60 mm, facing the center of the sample. The geometric model is shown in figures 19 and 20.

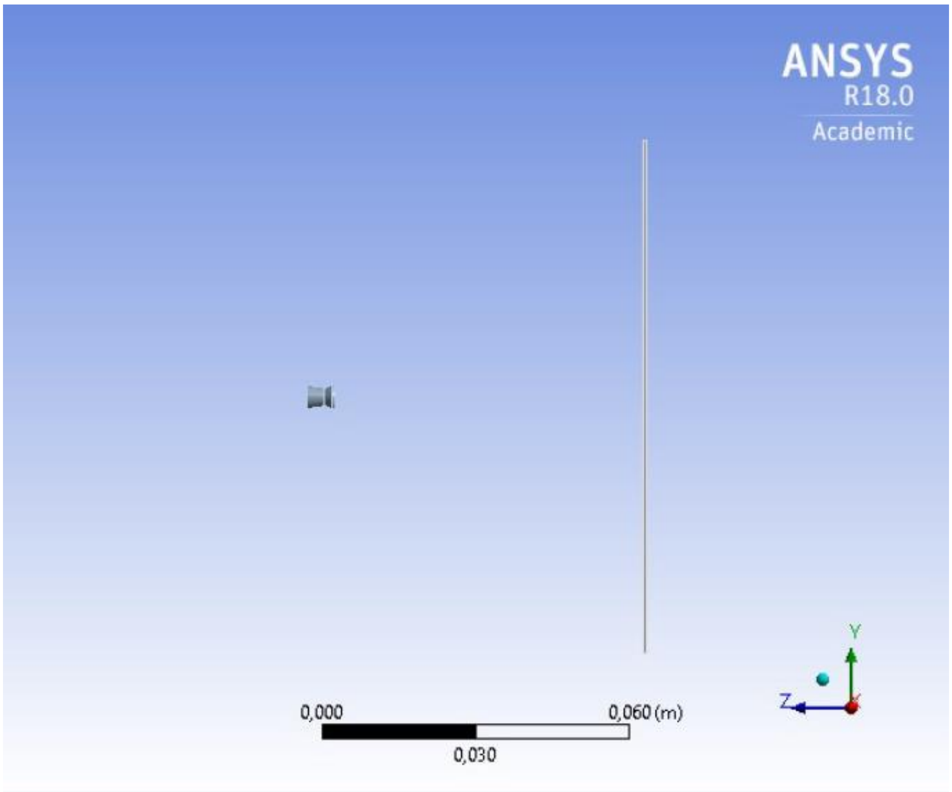

Figure 19 – The geometric model for the air gun impact numerical analysis in ANSYS Workbench, seen from the side

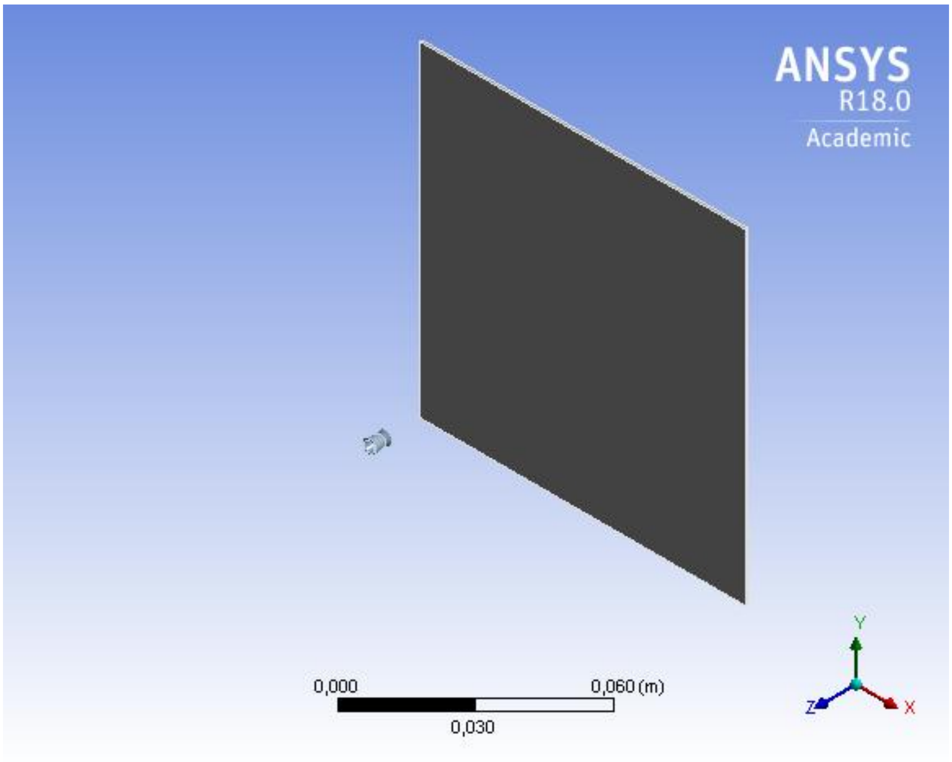

Figure 20 – The geometric model for the air gun impact numerical analysis in ANSYS Workbench, seen from an isometric view

The dimensions of the pellet are realistic dimensions of the Diabolo pellet used in the experimental test, and it measures 5,5 mm from front tip to back end.

The sample also have the same dimensions as the experimental test pieces, with a length and width of 100 mm. The thickness was first set to the single layer sample thickness of 0,79375 mm and then increased by for example x2 or x3 to match the thickness of the double layer and the triple layer samples accordingly, as seen in the experimental test. This was done to find the limiting thickness for penetration of the pellet.

To create a finite element (FE) model, an automated mesh was generated in ANSYS Workbench. The meshing of the model was limited by the number of elements/nodes allowed in the Academic license of ANSYS Structural physics, which is 32 000 nodes/elements. The highlighted mesh parameters are seen in table 3, for full list see Appendix B.

Table 3 – The mesh parameters for the FE model for the air gun impact analysis in ANSYS Workbench

Physics preference	Explicit
Relevance	70
Element Midside Nodes	Dropped
Relevance Center	Fine
Span Angle Center	Fine
Nodes	**9193**
Elements	**13786**

A mesh sensitivity analysis was performed by increasing the number of nodes and elements to see when the solution to the simulation converged. When a proper mesh was found, it was kept the same throughout all the tests with the different sample thicknesses, so that the mesh would not have an impact on the results obtained.

The material assigned to the CFRP sample was the Epoxy Carbon Woven (230 GPa) Wet, with pre-defined parameters in ANSYS. The material assigned to the Diabolo pellet was Lead, with pre-defined parameters in ANSYS. The parameters of both materials are shown in Appendix B.

A support was placed on all four sides of the CFRP sample to make sure it was constrained. A velocity of 160 m/s was set to the pellet in the negative z-direction.

The end time of the simulation was set to 7×10^{-4} seconds for the single layer and increased with increasing sample thickness to see the full impact reaction of the pellet and the sample.

The results of this analysis are presented and discussed in chapter 4.2.2.

3.3.3 Ice impact

To see how ice formation would impact the CFRP test pieces, a model was created for freezing ice on a device that could be shot out of the air gun. The model was created in Autodesk Inventor and 3D-printed by the CubePro Duo printers available in the Department of Engineering and Safety at UiT, as seen in figure 21.

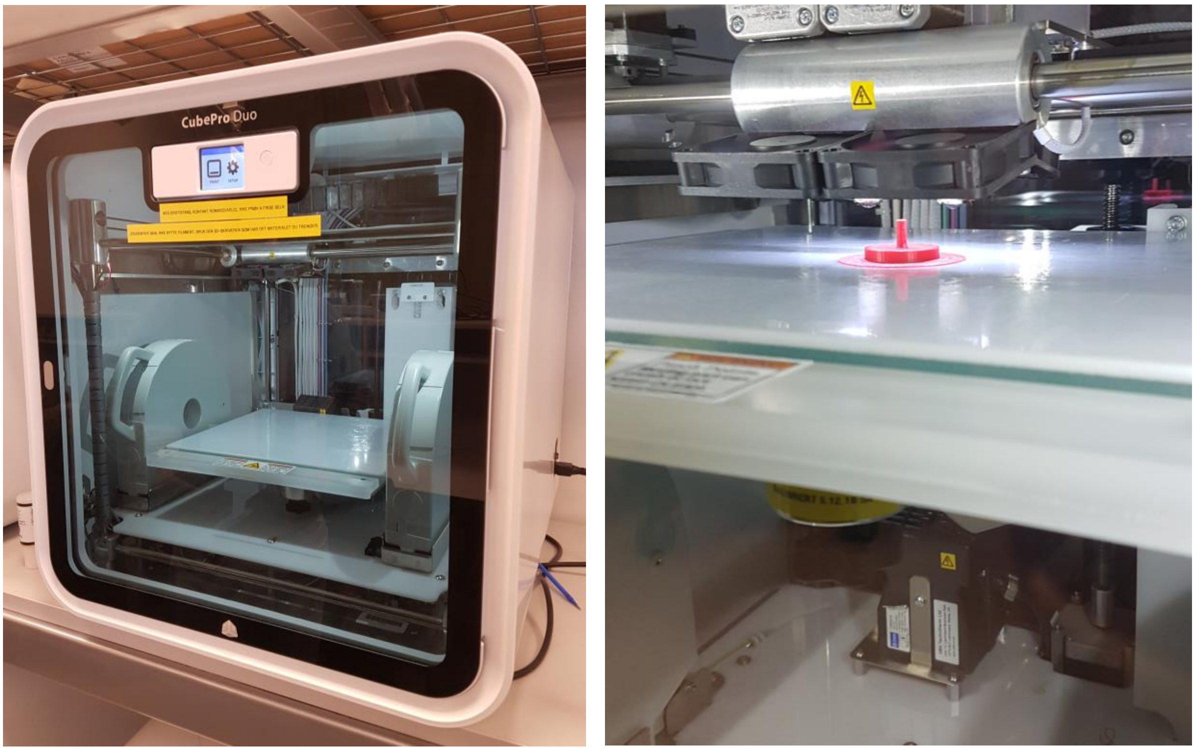

Figure 21 – The CubePro 3D printer used for printing ice impact testing device is seen to the left, and a picture taken while the device is being printed to the right.

The device is seen in figure 22 and consists of a cylindric extension that fits into the barrel of the air gun (a). On top of the extension a cylindric plate with shapes that allows the ice to freeze and adhere on to it (b). On top, a removeable cap to hold the water in contact with the cylindric plate while freezing (c).

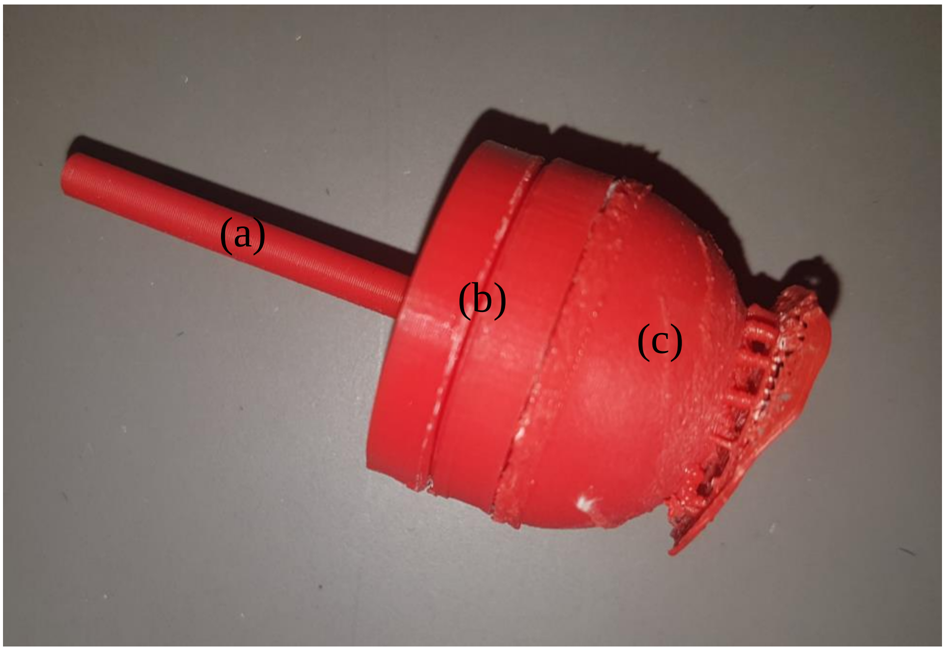

Figure 22 – The finished 3D printed device, with removeable cap.
(a) Cylindric extension that fits into the barrel of the gun,
(b) Cylindric plate with shapes (the shapes are hidden under the cap in this picture),
(c) Removeable cap to freeze the ice

A spherical shape of ice was frozen on to the cylindric plate, as seen in figure 23.

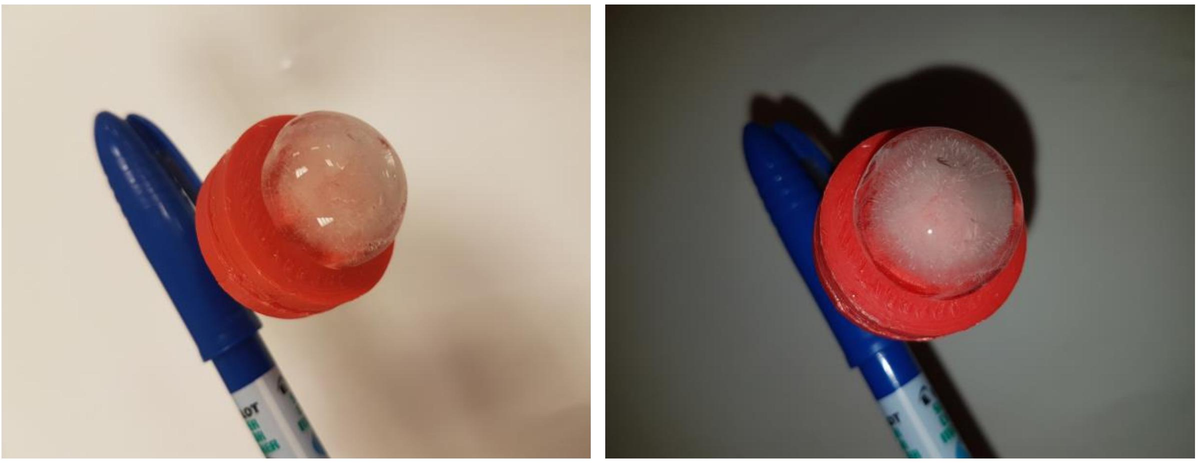

Figure 23 – The spherical shape of ice frozen on to the device. The pen is just for holding up the device for pictures.

With the device ready for experiments, it was attached into the barrel of the air gun as seen in figure 24. The cap was removed before shooting so that the ice would hit the CFRP test pieces directly.

Figure 24 – The device for shooting ice on the CFRP test pieces, attached to the air gun.

For this experiment the thin CFRP samples were cut into 100x100 mm test pieces to fit the hole on the shooting box. The box was placed standing up on a plane surface in the height of about 1,5 meters to allow for shooting horizontally.

The experiments were performed shooting with the air gun at a distance of a meter and half a meter.

3.4 Charpy impact

This study applies the Charpy impact test to the thick CFRP samples, as the thin samples are to bendable to break in the Charpy pendulum, which would have provided faulty results.

The given samples were cut into proper sized test pieces for the Charpy pendulum. According to the recommendation given by for example Bader and Ellis [20], based on their own experiments, the span-to-thickness ratio L_C/d should be 10 or more for trustworthy results.

In this project, samples with pre-dimensioned thickness d of 5 mm was provided. To meet the recommendations for the ratio L_C/d the only regulation to be made was the length L_C of the test pieces.

By measurements on the Charpy pendulum intended for the project, in addition to running tests with different lengths, a proper length L_C of 60 mm was found. This gives a span-to-thickness ratio L_C/d as shown in equation (3.23).

$$\frac{L_C}{d} = \frac{60\ mm}{5\ mm} = 12 \tag{3.23}$$

It should be noted that the width of the test pieces also could be regulated, but this dimension is not affecting the span-to-thickness ratio. While running the tests to find a proper length, different widths were also tested. The type of equipment to be used, and the preciseness in cutting the pieces, also had to be considered. A proper width of the test pieces was found to be about 5 mm. Because of errors during the cutting with a type of hand-held saw (wet tile cutter), all the pieces had a variation of width between 5-6 mm. The test pieces are unnotched.

The number of test pieces was limited to the number of available samples to cut from. A total of 60 test pieces were compiled. The 60 pieces were distributed to the three different types of tests to be performed:

- **Charpy impact test on test pieces of room temperature (about 22˚C)**
  The test was performed on 20 room temperate test pieces.
- **Charpy impact test on test pieces of cold temperature (about -20˚C)**
  The test was performed inside the cold room on 20 test pieces having stayed in the cold for one week to be sure the pieces had been temperate to the cold
- **Charpy impact test on circulated test pieces**
  The test was performed in room temperature on 20 test pieces that have been circulated in and out of the cold room 5 times. Starting in room temperature the circulating proceeded like this:
  - Room temperature	start-up
  - Cold room	30 min
  - Room temperature	30 min
  - Cold room	30 min
  - ….. continuing until the test pieces have been into the cold room 5 times.

The Charpy pendulum used for the Charpy tests is shown in figure 25.

Figure 25 – The Charpy pendulum used in this project

4 Results and discussion

The results are presented in different subchapters for each of the three types of test performed; the four-point bending test, the air gun impact test and the Charpy impact test. For the four-point bending test and the air gun impact test, there is also undersections which represents the experimental results and the numerical results. For the Charpy test, only experimental test has been performed, and therefore represented here with just the experimental results.

4.1 Four-point bending

4.1.1 Experimental results

The process of performing the experimental four-point bending test is thoroughly explained in chapter 3.2.1, but summed up briefly here;

Measurements were taken between the lower point of the upper frame and the upper point of the lower frame on all four corners. The value for deflection of the beam is the average of the four measurements.

Measurements were taken before applied weight and after applied weight. The applied weight was 16,3 kg (159,9 N).

The difference between the two measurements gives the deflection of the beam at the load points, and the results obtained are presented in table 4.

Table 4 – The obtained results of deflection of the beam in four-point bending

	Room temperate CFRP test pieces	CFRP test pieces being exposed to cold temperature for a week
Deflection of the beam (mm)	0,3475 (average of four readings)	0,605 (average of four readings)

The measurements should account for an error of +/- 0,005 mm due to measuring equipment sensitivity.

The deflection is slightly bigger on the test piece that has been exposed to the cold temperature for a week. This indicates that the CFRP may have softened or weakened a little due to the cold exposure.

4.1.2 Numerical results

When a displacement of 0,3475 mm is applied to the load points, the obtained resultant force in negative z-direction is 142,42 N. (Appendix A)

The total deformation of the beam is seen in figure 26.

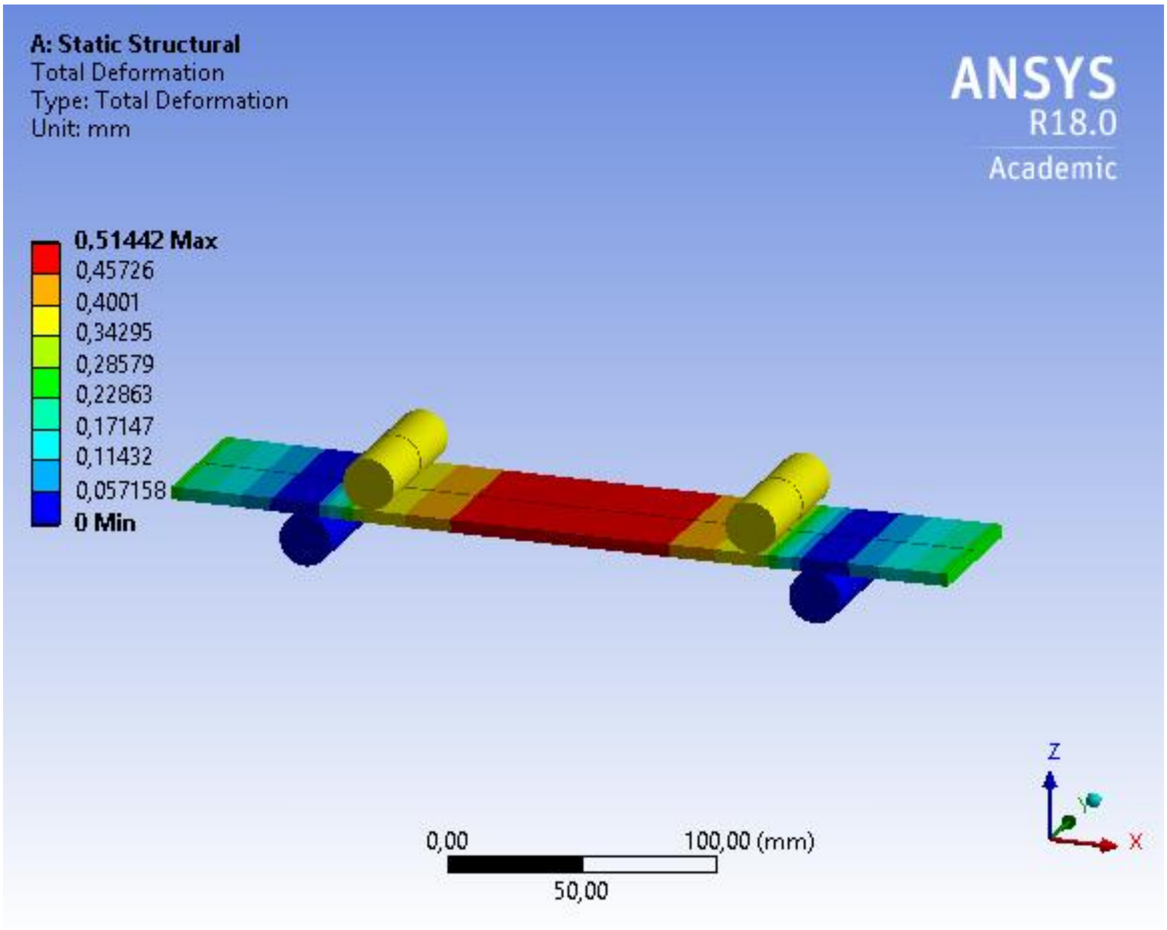

Figure 26 – The total deformation of the beam

The deflection of the beam in the z axis is seen in figure 27.

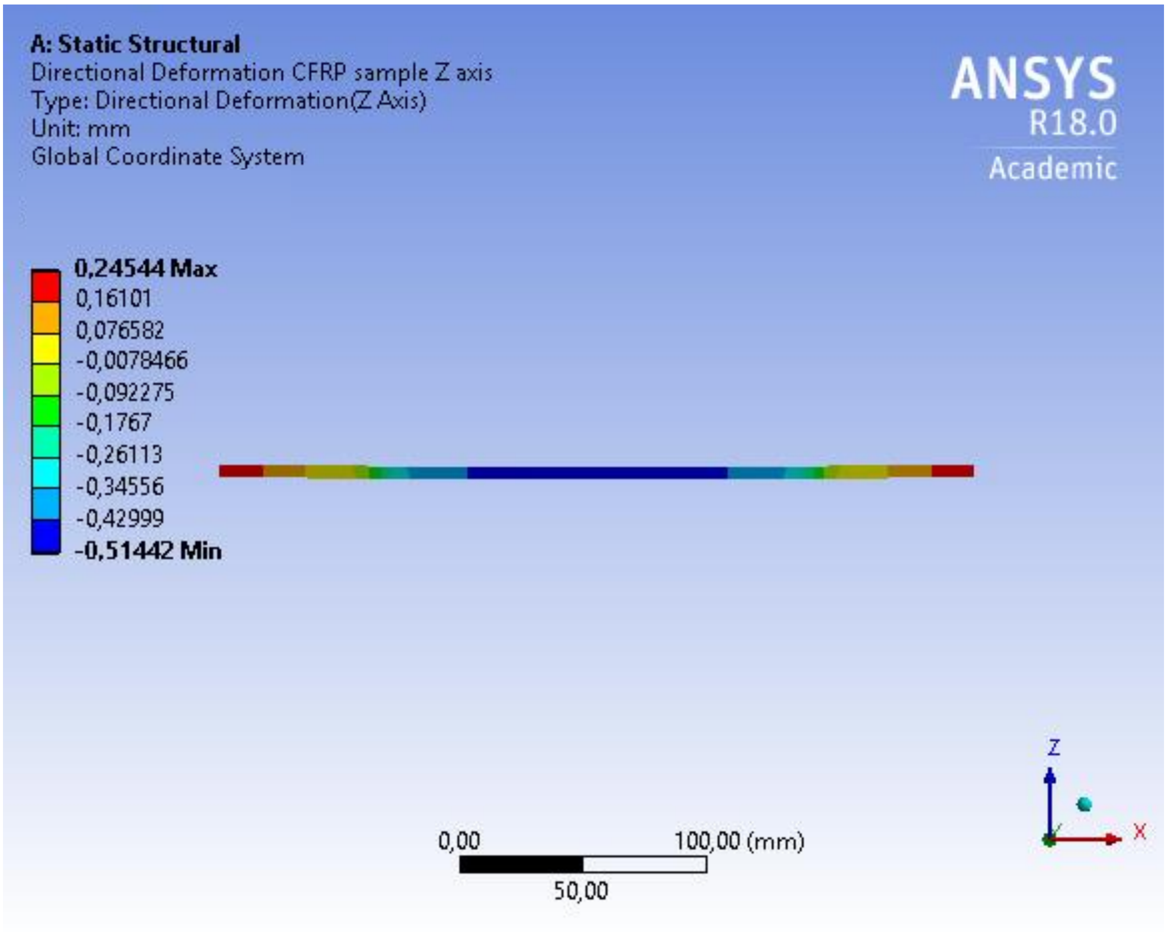

Figure 27 – The deflection of the beam in the z axis.

From the experimental results, it was found that a force in negative z-direction of 159,9 N is needed to obtain a deflection of 0,3475 mm.

This means that there is a difference of 17,48 N (11%) between the experimental and the numerical results. This verifies that the material used for the CFRP samples in the numerical analyses are right according to the CFRP samples provided for this project.

4.2 Air gun impact

4.2.1 Experimental results

The visual results of the impact failure mode of shooting through a single layer test piece with a thickness of ~0,79 mm is shown in figure 28, shot with Diabolo pellet (a) and Storm pellet (b). Both types of pellets have passed right through the test piece, leaving different shaped holes only. The carbon fibers in the CFRP have been torn off from each other leaving the material scattered out in all directions without cutting off at the back end.

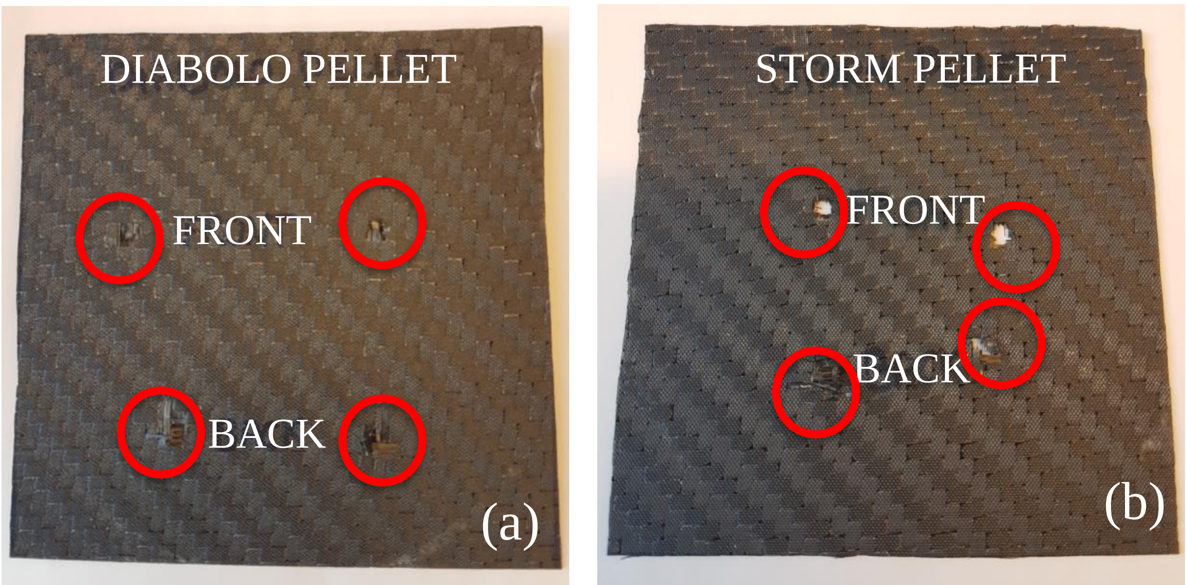

Figure 28 – A visual display of the impact failure mode of shooting through a single layer test piece with an air gun, with Diabolo pellets (a) and Storm pellets (b).

The results of the permeability test performed in room temperature is shown in figure 29, with the Diabolo pellet (a) and the Storm pellet (b). Both types of pellets have only penetrated a single layer of the CFRP test pieces. At the double layered sequence, the pellet has stopped and left residual on the layer, but not passing through. This shows that the CFRP samples are permeable at single layer, but not when doubled up to two layers. The test is therefore not performed further on 3-4 layers.

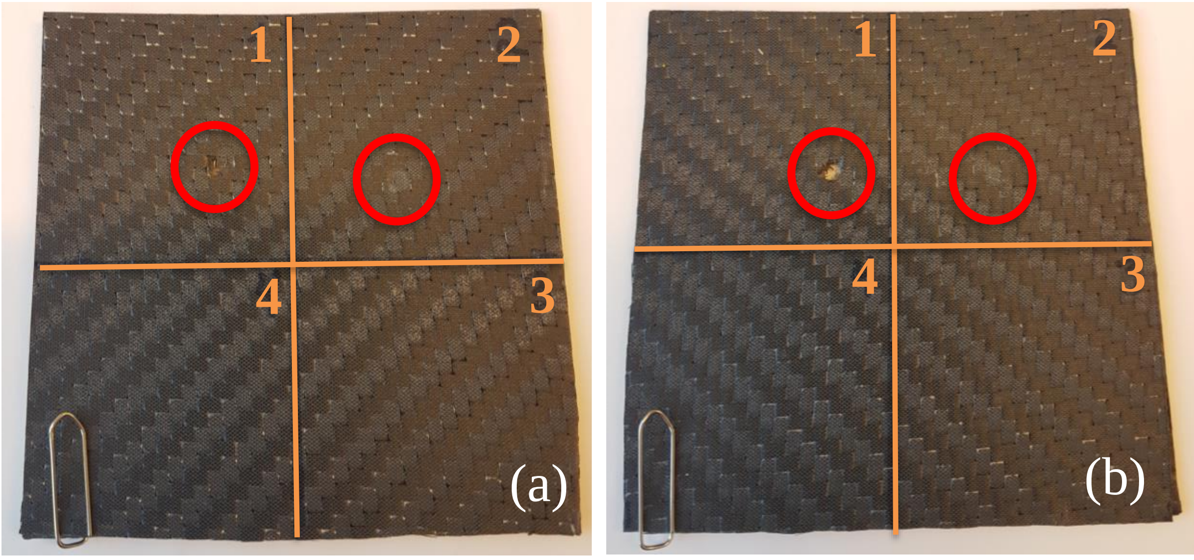

Figure 29 – A visual display of the impact failure mode of shooting through (or onto) different number of layers of CFRP test pieces with an air gun with Diabolo pellets (a) and Storm pellets (b). The number of layers are defined by the number inside the squared sequences of the test piece in the front.

The results of the permeability test performed in the cold room on test pieces exposed to about -28˚C for one week is shown in figure 30. The results are the same as the results of the permeability test on room temperate test pieces. Both types of pellets have penetrated a single layer of the CFRP test piece, and stopped at the double layered sequence.

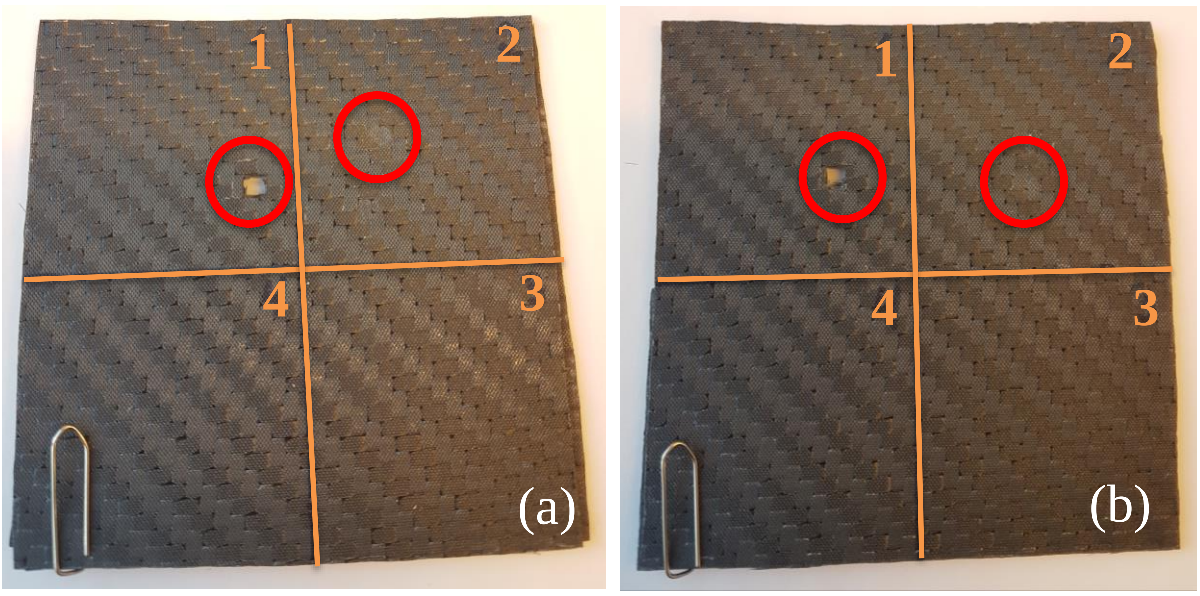

Figure 30 – A visual display of the impact failure mode of shooting through (or onto) different number of layers of CFRP test pieces with an air gun with Diabolo pellets (a) and Storm pellets (b). The number of layers are defined by the number inside the squared sequences of the test piece in front.

This shows that the permeability of the CFRP samples are the same after being exposed to cold temperature.

However, it should be noted that the experimental results are limited to tell the number of layers needed for the pellet to not be able to penetrate, and it is not possible to determine the exact thickness (between single and double layer) where the pellet is being stopped. The numerical results are suitable to find this value.

It should be noted, since the experimental results showed similar results for room temperature and cold temperature tests, the numerical tests are performed only with a room temperature environment.

4.2.2 Numerical results

The obtained deformation results of the simulation with a sample thickness of ~0,79 mm (single layer), seen from the side (from the positive x-direction) is shown in figure 31. The pellet has impacted the sample (a), created a hole (deleted elements) and passed through it (b), which means failure has occurred. This behavior is in accordance with the experimental results of the single layer.

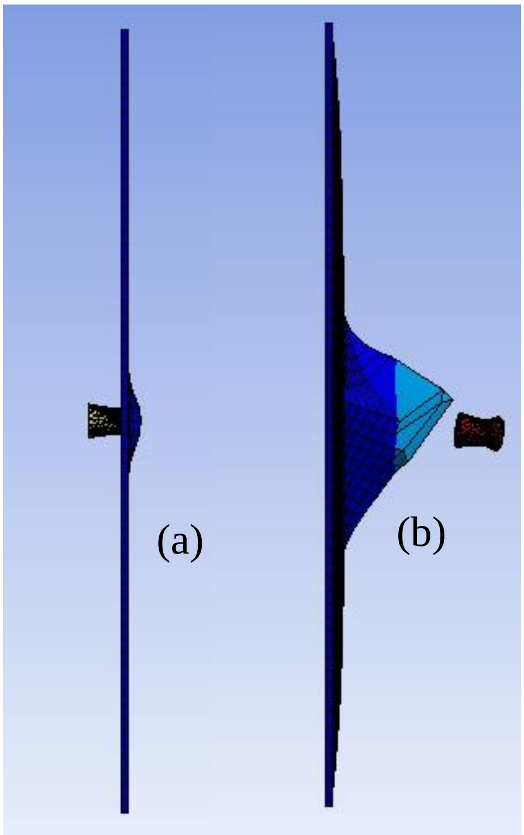

Figure 31 – The obtained results of the single layer simulation in ANSYS Workbench, seen from the side (from the positive x-direction)

The deformation result of the same single layer sample simulation, seen from the front (from the positive z-direction) of the sample is shown in figure 32.

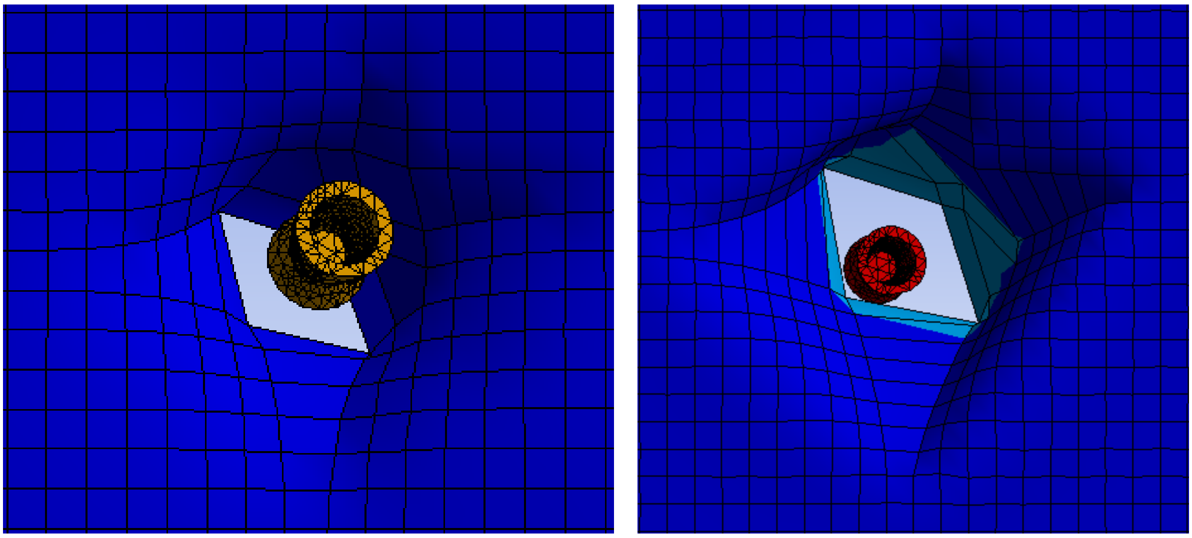

Figure 32 – The obtained results of the single layer simulation in ANSYS Workbench, seen from the front of the sample (from the positive z-direction)

The deformation result of the same single layer sample simulation, seen from the back (from the negative z-direction) of the sample is shown in figure 33.

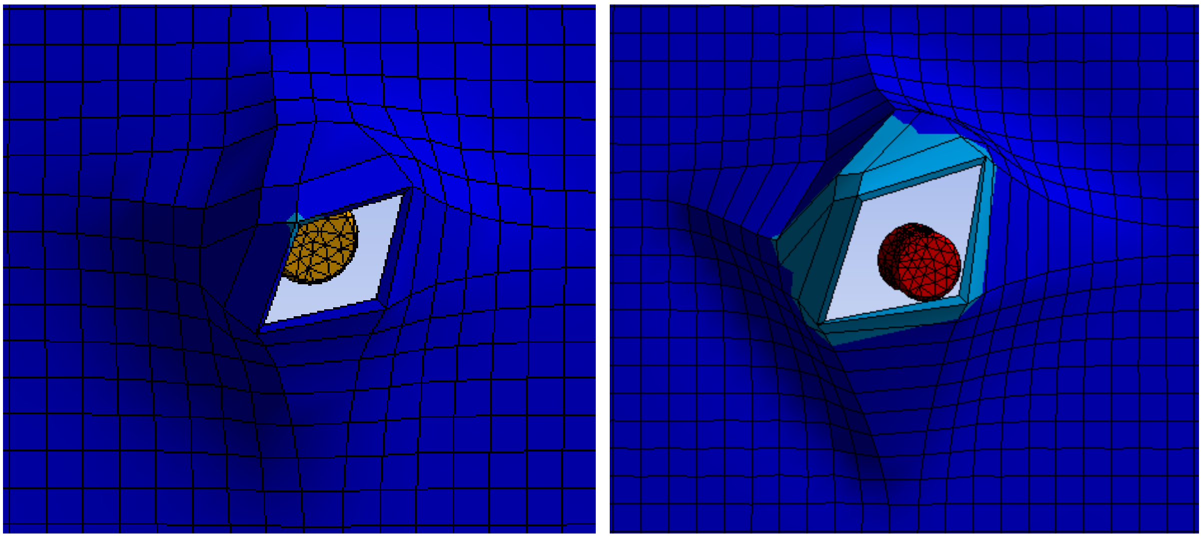

Figure 33 – The obtained results of the single layer simulation in ANSYS Workbench, seen from the back of the sample (from the negative z-direction).

Since the simulation shows that the pellet can penetrate a sample thickness of ~0,79 mm (single layer), the thickness of the sample was doubled to ~1,59 mm, which equals the experimental double layer.

The obtained deformation results of the simulation with a sample thickness of ~1,59 mm (double layer) seen from the side (from the positive x-direction) is shown in figure 34. The pellet impacts the sample (a), creates a maximum deformation of the sample (b), and then bounces back (c).

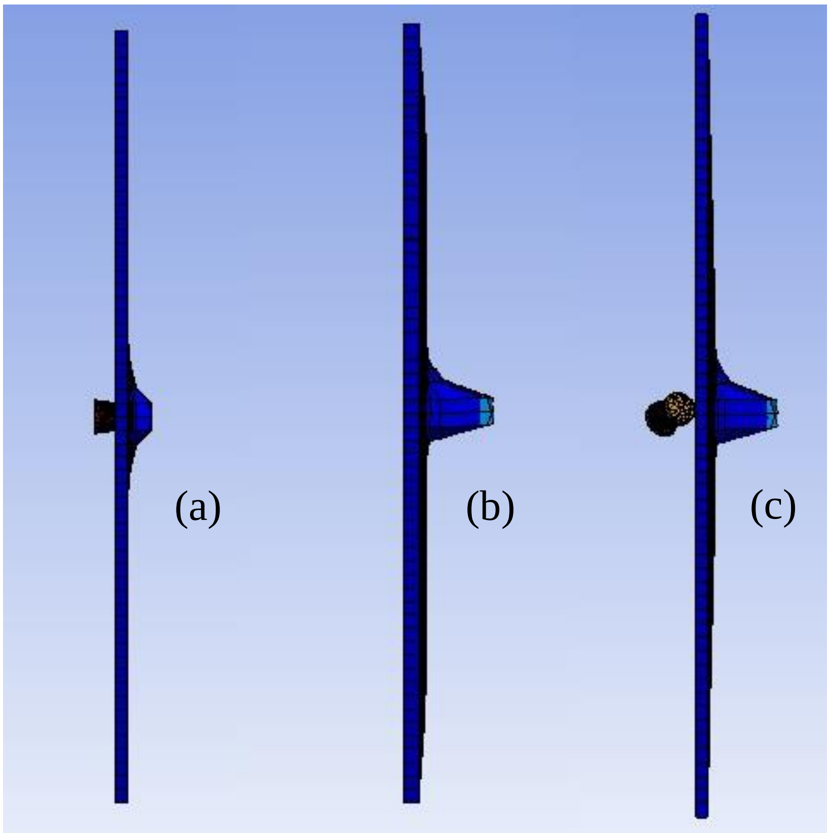

Figure 34 – The obtained results of the double layer simulation in ANSYS Workbench, seen from the side (from the positive x-direction)

In figure 35, the impact is seen from the front (a) (from the positive z-direction) and from the back (b) (from the negative z-direction) of the sample. A failure has occurred, and a hole is created in the sample (deleted elements).

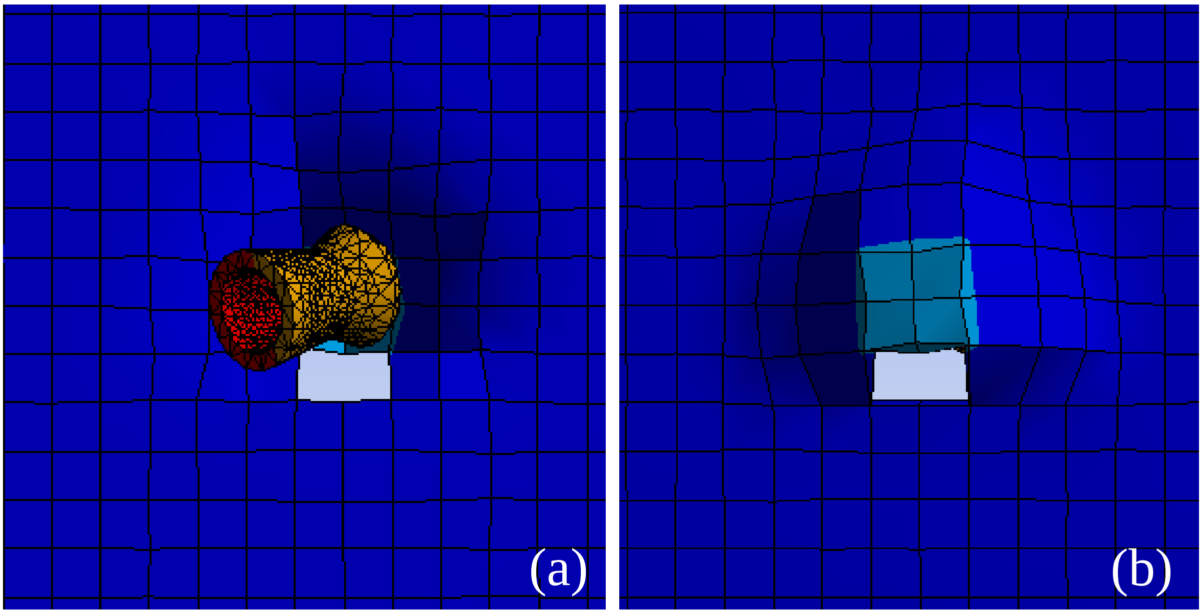

Figure 35 – The obtained results of the double layer simulation in ANSYS Workbench, seen from the front of the sample (a) (from positive z-direction) and from the back of the sample (b) (from the negative z-direction).

The result of the double layer simulation is not in accordance with the experimental results. From the experimental results the pellet could not penetrate the test piece, nor did it impact or create any failures to it, other than leaving residuals from the pellet itself.

Even though the pellet visually did not penetrate the sample in the numerical test, a failure occurred in the form of deleted elements. When this is transferred to "the real life" it is reasonable to think that the carbon fibers of the CFRP samples has opened up and scattered out in the same way as seen in the single layer results in chapter 4.2.1, making it possible for the pellet to actually penetrate the sample.

Since the numerical result does not match the experimental result it should be kept in mind that the buildup of layers is done different in the two types of tests. In the experiments, the thin CFRP samples were laid up on each other to create the double layer, the triple layer and so on. In the numerical test in ANSYS Workbench, the CFRP sample were created as one sample (one body), starting with a thickness identical to the thin CFRP samples, and then creating double layer by increasing the thickness by 2. This means that in the experiment there is a marginally thin gap of air in between each layer, which is not considered in the numerical test.

As the numerical results revealed that the pellet in theory could penetrate a double layer sample, the thickness was tripled to ~2,38 mm (~0,79 mm x 3) in the next simulation. The obtained deformation results of the simulation with this thickness, seen from the side (from the positive x-direction) is shown in figure 36. The pellet impacts the sample (a), leaving a deformation, then bounces back (b).

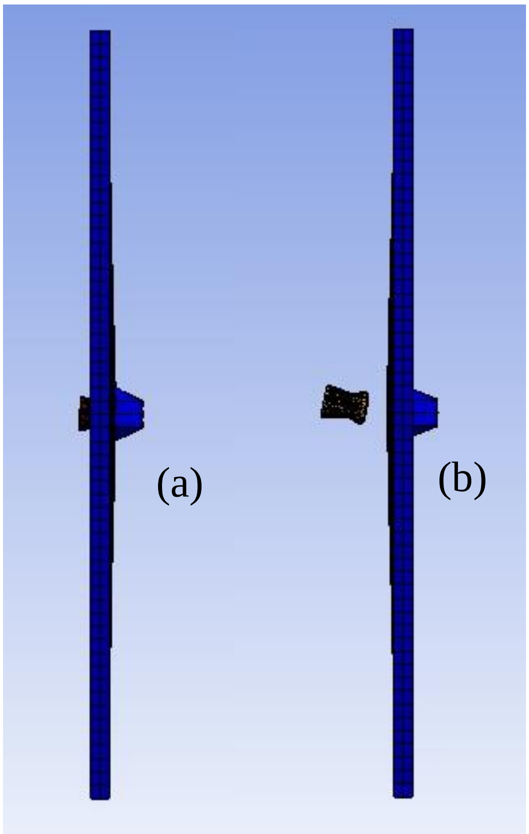

Figure 36 – The obtained results of the triple layer simulation in ANSYS Workbench, seen from the side (from the positive x-direction).

In figure 37 the impact is seen from the front (a) (from the positive z-direction) and from the back (b) (from the negative z-direction).

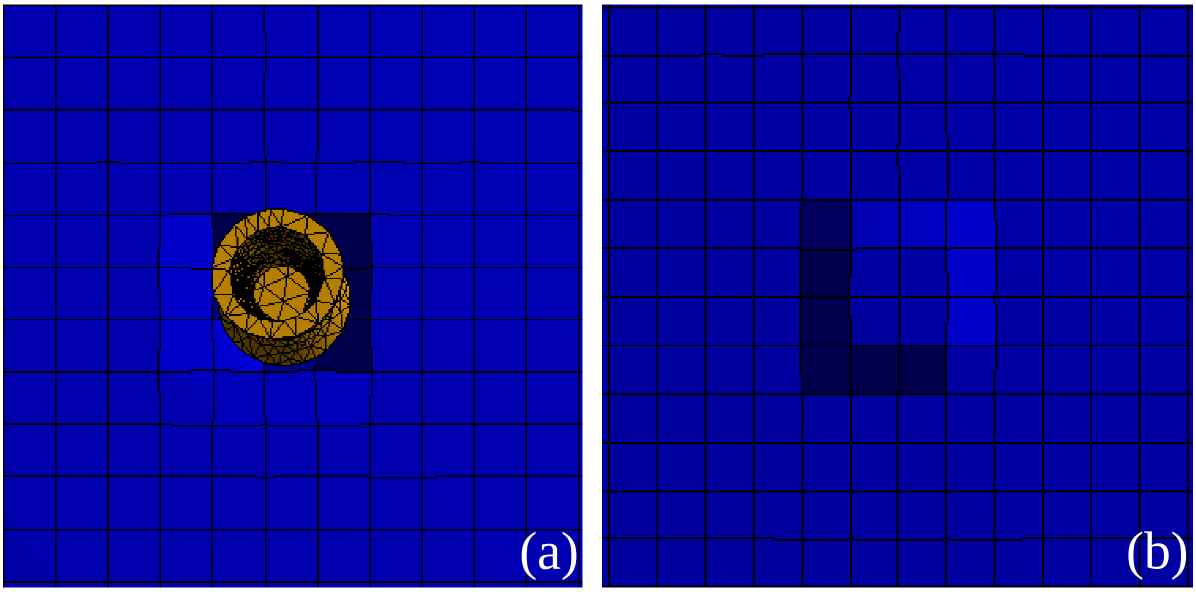

Figure 37 – The obtained results of the triple layer simulation in ANSYS Workbench, seen from the front of the sample (a) (from positive z-direction) and from the back of the sample (b) (from the negative z-direction).

The impact has not made any visual failures like a hole of deleted elements to the sample. This means, according to the numerical results, the pellet cannot penetrate triple layer sample.

So far, the numerical results have shown that the limiting thickness for penetration is somewhere between double layer thickness of ~1,59 mm and triple layer thickness of ~2,38 mm.

With this information, the numerical analysis was continued with different sample thickness decreasing from the triple layer thickness down to the double layer thickness, trying to find the exact thickness where penetration happens.

At a thickness of ~1,63 mm (which is the single layer thickness times 2,05), there were still no failure/holes in the sample, only the same deformation as seen in the triple layer sample. This is seen in figure 38, with the impact from the front (a) (from the positive z-direction) and from the back (b) (from the negative z-direction).

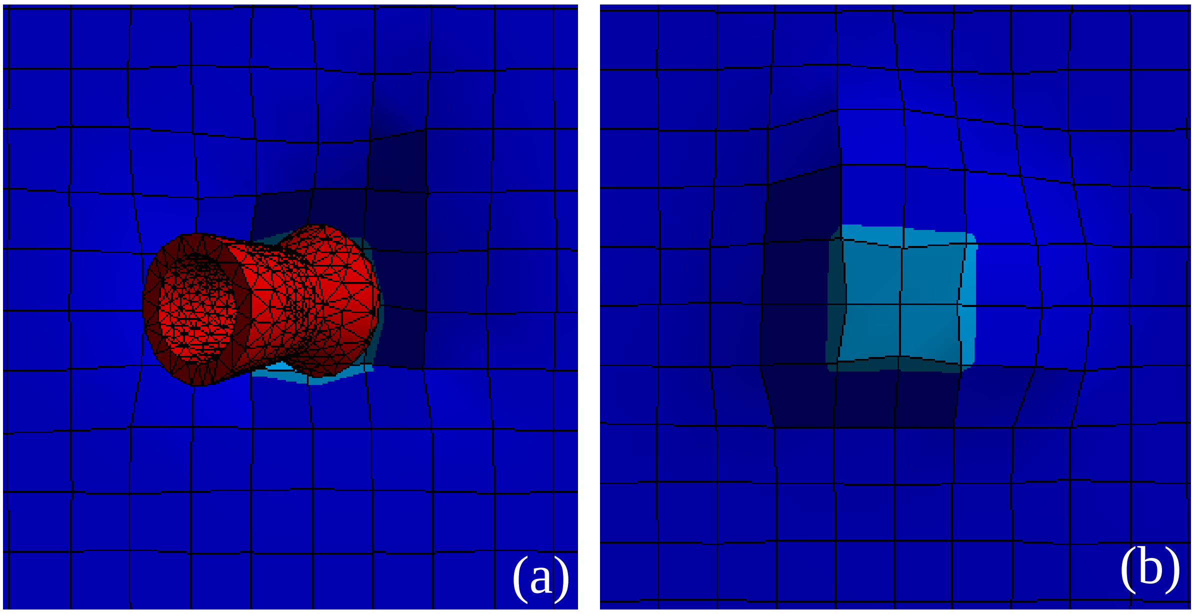

Figure 38 – The obtained results of the ~1,63 mm thickness sample simulation in ANSYS Workbench, seen from the front of the sample (a) (from positive z-direction) and from the back of the sample (b) (from the negative z-direction).

Therefore, it was concluded that the limiting thickness for penetration, as found in the numerical analysis, is in the range between ~1,59 mm and ~1,63 mm.

4.2.3 Summary of experimental and numerical results

Because the experimental results and the numerical results obtained from the air gun impact test shows differences, all results are summed up in table 5, where the x indicates penetration of the pellet through the sample at the given thickness, and – indicates no penetration.

Table 5 – A summary of the results obtained from the experimental and the numerical air gun impact test.

	Experimental result	**Numerical result**
Single layer **~0,79 mm**	x	x
In the range between single and double layer **~0,79 mm - ~1,59 mm**	x	x
Double layer **~1,59 mm**	-	x
In the range between double layer and single layer x 2,05 **~1,59 mm - ~1,63 mm**	-	x
In the range between single layer x 2,05 and triple layer **~1,63 mm - ~2,38 mm**	-	-
Triple layer **~2,38 mm**	-	-

4.2.4 Ice impact

The set-up for the ice impact test has been described under chapter 3.3.3. Summed up, ice was frozen onto the 3D-printed device to form a spherical shape. The device was placed into the barrel of the gun. The test samples, cut into 100x100 mm test pieces to fit the hole in the shooting box, were fastened to the box, and the box was standing up on a plane surface in the height of about 1,5 meters, to allow for shooting horizontally.

The device with ice on, were shot from the air gun with a distance to the test piece of first one meter, and in second try, half a meter.

The results of the air gun impact test with the use of the 3D-printed ice-device shows that the impact of ice shoot onto the CFRP test pieces did not make any visible changes in the material of the test pieces, nor any deformation. It should be noted that this result is based only on visual inspection, no instruments for detection or measuring of deformation were used.

Based on this results, a decision was made to not perform any further studies of the ice impact in this project and the report, even though the test result is mentioned briefly here so it can be noted by the reader.

4.3 Charpy impact

Summed up, the Charpy impact tests were performed on test pieces with three different temperature settings:

- Charpy impact test on test pieces of room temperature (about 22˚C)
- Charpy impact test on test pieces of cold temperature (about -20˚C)
- Charpy impact test on circulated test pieces

Each type of test had 20 test pieces designated to them, 60 pieces in total. During the testing, unrealistic high numbers was discarded, along with the tests that gave faulty results for other reasons (human error in operation with the Charpy pendulum). The three different tests gave 18 valid test results each, a total of 54. This means that the average in the quantitative results is calculated from 18 test runs at each temperature setting.

The qualitative results are presented in table 6 (Appendix D), and they are independent of temperature.

Table 6 – The qualitative results of the Charpy test

	Cut off (Fiber-dominated failure)	Delamination (Matrix-dominated failure)	Total
Number of failures #	13	41	54
Percentage %	24	76	100

A visual display of the two types of failures is shown in figure 39. The results show a domination of delamination failures (a) which indicates failure in the matrix. Cut off failures (b) which indicates failure in the fibers are underrepresented.

Figure 39 – A visual display of the qualitative results of the Charpy test

It should be noted that even if test piece (b) has been cut in two, some delamination has also happened in the layers close to the cut during the impact process.

The quantitative results of the Charpy impact test is shown in table 7 (Appendix D).

Table 7 – The quantitative results of the Charpy test

	Highest reading (Nm)	**Lowest reading (Nm)**	**Average (Nm)**	**Standard Deviation (Nm)**
Room temperature (about 22 ˚C)	8,34	3,83	**5,89**	**1,34**
Cold room (about -20 ˚C)	8,04	3,34	**5,31**	**1,53**
Cyclic	8,53	02,94	**5,36**	**1,63**

The results are given in Nm. The direct reading from the Charpy pendulum is on the other hand given in kpm. The equation for converting from kpm to Nm is given:

$$1\ kpm \times 9{,}81\ \frac{m}{s^2} = 9{,}81\ Nm$$

The results are showing that the average amount of energy that the CFRP samples can absorb before failure occurs is 5,89 Nm in room temperature, with a standard deviation of 1,34 Nm. After one week in the cold room at about -20 ˚C the rate of energy absorption has dropped by 9,85% to 5,31 Nm, with a standard deviation of 1,53. The result after the cyclic exposure to the cold room also shows a drop in the rate of energy absorption by 9% to 5,36 Nm, with a standard deviation of 1,63.

The difference in the average value between the exposure to cold room for one week and the cyclic exposure to the cold room is of 0,05 mm and that is a negligible difference in this matter.

That means that a general exposure to cold temperatures weakens the CFRP samples by about 9-10% even after a short time. However, it is important to note that the experimental results had a significant standard deviation. This was because of the quality of the test pieces, the cutting process, etc. Nonetheless the above finding is reasonable for the engineering design studies.

5 Summary and Conclusion

From the four-point bending test, a slightly bigger deflection was found in the CFRP samples exposed to cold temperature, compared to the room temperate test pieces, meaning that the exposure to the cold has softened/weakened the CFRP samples.

When the experimental results of four-point bending on the room temperate CFRP test pieces were compared to the numerical results, a difference of 17,48 N was seen. For the engineering design studies, this difference is insignificant, and the result verifies that the material used for the numerical analyses are comparable with the actual CFRP samples provided for this project.

From the air gun impact test, the limiting thickness for penetration in the CFRP samples were found to be slightly different in the experiments and the numerical test. From the experimental results, it was concluded that the limit exists somewhere in the range between ~0,79 mm and ~1,59 mm, which equals the range of thickness between single layer and double layer sample. This result was the same for samples exposed to cold temperature and the room temperate samples. From the numerical results, it was concluded that the limit exists somewhere in the range between ~1,59 mm and ~1,63 m, which equals the range of thickness between single layer sample thickness and single layer x 2,05 sample thickness.

Summed up, this means that the limiting thickness for penetration is in the range between ~0,79 mm and ~1,63 mm, and the result is the same in the samples exposed to the cold temperature and the room temperate samples.

From the Charpy impact test, it was found that a general exposure to cold temperatures weakens the CFRP samples by about 9-10% even after a short time.

By looking at all the results, it is reasonable to conclude that the strength of the CFRP samples decreases some, when exposed to the cold. It is hard to state exactly how much, but an estimate of about 10% decrease in strength seems realistic.

6 Challenges

Some minor and major challenges were faced during the work with this project, and they are briefly explained here.

- **Limited amount of CFRP samples provided for the project**
  It was provided 6 thin samples and 2 thick samples for this project, all of them about 300x300 mm in size. This limited the amount of test pieces that could be cut out of the samples, and this again limited the number of tests.

- **Limitations in available equipment**
  The equipment available for this project was limited to what was available in the university, in addition to the equipment that could be bought for the 5500 NOK granted for the project, by the university. One major challenge in the beginning was to find equipment for cutting the samples into smaller test pieces. Different kind of scissors were first tried, all from regular ones to more advanced handheld scissors. It was found that a metal scissor worked quite OK for the thin samples, but for the thick samples, something more advanced was necessary. After trying out different types of cutters and saws, it was found that a wet tile cutter could do the work quite nicely. It should be noted though, that HSE concerns needs to be considered for cutting carbon fiber. It creates sharp edges of splint fibers and particulate matter that could be unhealthy or dangerous.

  This challenge took quite a lot of time and effort to figure out in the beginning of the project. Also, the cutting it selves took a good portion of time because of the HSE concerns. This delayed the start-up time for the experiments.

  The equipment for performing the tests was also limited in the university. The only test device available, relevant for this project was the Charpy pendulum. The four-point bending test device had to be built by hand from scratch. The shooting box for the air gun impact test was also constructed to provide for safety under the experiment.

- **Computer problems**

  It was a challenge to run the simulations in ANSYS Workbench on a regular private computer because it could not handle the computational load of the simulations. When the supervisor was made aware that a lot of students using ANSYS for their project were struggling with the same problem, the decision was made in the university to order in some computers (Lenovo P910) with the ability of solving big problems in ANSYS. These computers arrived at the beginning of May. So, the simulations presented in this report were carried out in May, with less than 1 month left to due date for the MS thesis.

- **Cold room temperature**

  Students have no option to control the temperature in the cold room. The temperature is being controlled externally. Other people are also using the cold room frequently and factors as opening and closing of the door will have short term effects on the temperature. However, the temperature is assumed to be held between -10˚C and -30˚C.

7 Future work

Time and resources was limited in this project. It is possible to expand the work presented in this report or build new projects with basis in this project. A few suggestions of future work are presented here:

- With more CFRP samples available it is possible to perform the experiments in a larger scale, with more test runs.

- Comparison of different types of CFRP samples, for example a comparison of the characteristics of quasi-isotropic samples with the characteristics of non-quasi-isotropic samples.

- Perform more types of tests if equipment is available, for example a tensile test.

References

1. ACMA. *Composites*. 2017 [cited 01.02.2017]; Available from: http://www.acmanet.org/composites.

2. Cha, K.K., *Composite Materials: Science and Engineering*. 2013: Springer New York.

3. Chung, D.D.L. and D. Chung, *Carbon Fiber Composites*. 2012: Elsevier Science.

4. *Composites push ahead in aerospace.* Reinforced Plastics, 1998. **42**(1): p. 50-54.

5. Dr. S. Selvaraju, S.I., *Applications of composites in marine industry.* Journal of Engineering Research and Studies, 2011.

6. Alan T. Nettles, A.J.B., *Low Temperature Mechanical Testing of Carbon-Fiber/Epoxy-Resin Composite Materials.* 1996. **NASA Technical Paper 3663**.

7. *Composites*, in *The Essential Chemical Industry Online*. 2013, The University of York.

8. Dutta, P.K., *Behavior of materials at cold regions temperatures Part 1: Program rationale and test plan*, in *Special Report 88-9*. 1988: US Army Corps of Engineers Cold Regions Research & Engineering Lab.

9. Lubin, G., *Handbook of Composites*. 2013: Springer US.

10. Gibson, R.F., *Principles of Composite Material Mechanics*. 1994: McGraw-Hill.

11. *MBI Mar-Bal Incorporated - History of Composite Materials*. [cited 26.05.2017]; Available from: http://www.mar-bal.com/language/en/applications/history-of-composites/.

12. *ACMA compositeslab - History of composites*. [cited 26.05.2017]; Available from: http://compositeslab.com/composites-101/history-of-composites/.

13. Bulmanis, V.N., et al., *Atmospheric durability of polymer-fiber composites in cold climates.* Mechanics of Composite Materials, 1991. **27**(6): p. 698-705.

14. Gao, S.-L. and J.-K. Kim, *Cooling rate influences in carbon fibre/PEEK composites. Part III: impact damage performance.* Composites Part A: Applied Science and Manufacturing, 2001. **32**(6): p. 775-785.

15. Kasen, M.B., *Composite Reliability*. 1975: American Society for Testing and Materials.

16. Vollen, Ø., *Mekanikk for ingeniør - Statikk og Fasthetslære*. 1999: nki forlaget.

17. Roylance, D., *Mechanical properties of material*. 2008.

18. Kato, H., Y. Tottori, and K. Sasaki, *Four-Point Bending Test of Determining Stress-Strain Curves Asymmetric between Tension and Compression.* Experimental Mechanics, 2014. **54**(3): p. 489-492.

19. TWI. *What is Charpy testing?* [cited 31.05.2017]; Available from: http://www.twi-global.com/technical-knowledge/faqs/material-faqs/faq-what-is-charpy-testing/.

20. M. G. Bader, R.M.E., *The effect of notches and specimen geometry on the pendulum impact strength of uniaxial cfrp.* Composites, 1974: p. 253-258.

21. Tanks, J., S. Sharp, and D. Harris, *Charpy impact testing to assess the quality and durability of unidirectional CFRP rods.* Polymer Testing, 2016. **51**: p. 63-68.

22. Logan, D.L., *A First Course in the Finite Element Method*. 2011: Cengage Learning.

23. *Allred and Associates Inc - Company*. [cited 09.03.2017]; Available from: http://dragonplate.com/sections/company.asp.

24. *Allred and Associates Inc - Product*. [cited 09.03.2017]; Available from: http://dragonplate.com/ecart/product.asp?pID=5749&cID=201.

25. *Allred and Associates Inc - Quasi-isotropic*. [cited 06.05.2017]; Available from: https://dragonplate.com/ecart/categories.asp?cID=65.

26. Khawaja, H.X.H., *Analytical and case studies of a sandwich structure using Euler-Bernoulli beam equation.* MESA, 2016. **Vol. 7, No. 4**: p. 599-612.

Appendix A – ANSYS Workbench data of the four-point bending test

Project

First Saved	Tuesday, February 21, 2017
Last Saved	Tuesday, May 23, 2017
Product Version	18.0 Release
Save Project Before Solution	No
Save Project After Solution	No

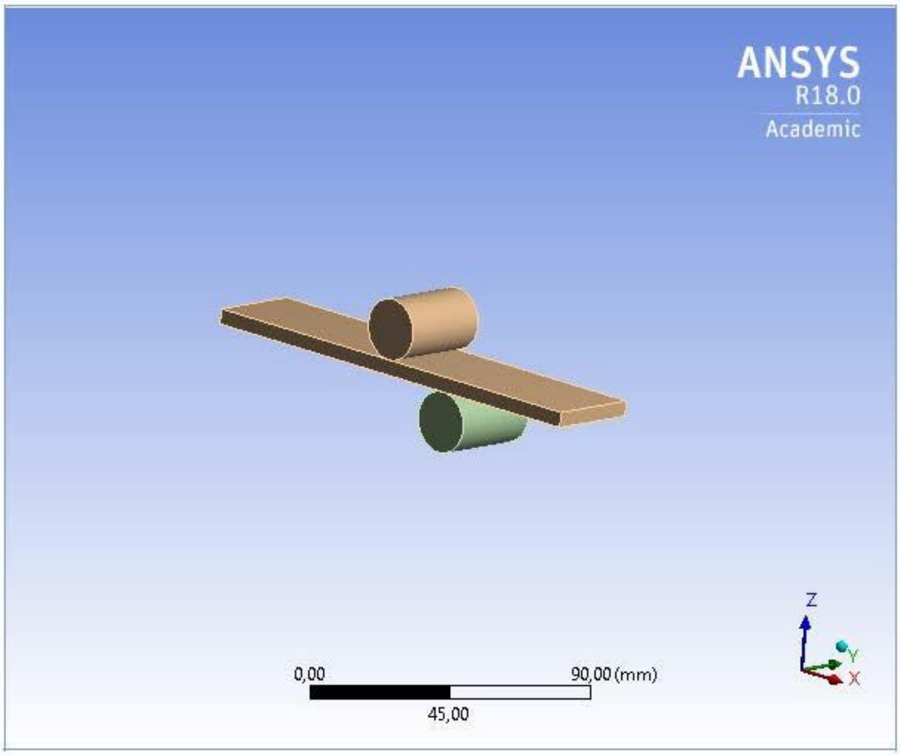

Contents

Report Not Finalized

Not all objects described below are in a finalized state. As a result, data may be incomplete, obsolete or in error. View first state problem. To finalize this report, edit objects as needed and solve the analyses.

Units

TABLE 1

Unit System	Metric (mm, kg, N, s, mV, mA) Degrees rad/s Celsius
Angle	Degrees
Rotational Velocity	rad/s
Temperature	Celsius

Model (A4)

Geometry

TABLE 2
Model (A4) > Geometry

Object Name	*Geometry*
State	Fully Defined

Definition	
Source	C:\ANSYS local files\Cathrine\Bending\CFRP Four point bending_files\dp0 \SYS\DM\SYS.agdb
Type	DesignModeler
Length Unit	Meters
Element Control	Program Controlled
Display Style	Body Color
Bounding Box	
Length X	152,4 mm
Length Y	30, mm
Length Z	45, mm
Properties	
Volume	41710 mm³
Mass	0,18114 kg
Scale Factor Value	1,
Statistics	
Bodies	3
Active Bodies	3
Nodes	29031
Elements	24750
Mesh Metric	None
Basic Geometry Options	
Parameters	Independent
Parameter Key	
Attributes	Yes
Attribute Key	
Named Selections	Yes
Named Selection Key	
Material Properties	Yes
Advanced Geometry Options	
Use Associativity	Yes
Coordinate Systems	Yes
Coordinate System Key	
Reader Mode Saves Updated File	No
Use Instances	Yes
Smart CAD Update	Yes
Compare Parts On Update	No
Attach File Via Temp File	Yes
Temporary Directory	C:\Users\cst037\AppData\Roaming\Ansys\v180
Analysis Type	3-D
Decompose Disjoint Geometry	Yes
Enclosure and Symmetry Processing	Yes

TABLE 3
Model (A4) > Geometry > Parts

Object Name	*CFRP*	*Solid*	*Solid*
State	Meshed		
Graphics Properties			
Visible	Yes		
Transparency	1		
Definition			

Suppressed	No		
Stiffness Behavior	Flexible		
Coordinate System	Default Coordinate System		
Reference Temperature	By Environment		
Behavior	None		
Material			
Assignment	Epoxy Carbon Woven (230 GPa) Wet	Structural Steel	
Nonlinear Effects	Yes		
Thermal Strain Effects	Yes		
Bounding Box			
Length X	152,4 mm	20, mm	
Length Y	30, mm		
Length Z	5, mm	20, mm	
Properties			
Volume	22860 mm³	9424,8 mm³	
Mass	3,317e-002 kg	7,3985e-002 kg	
Centroid X	76,2 mm	100, mm	75, mm
Centroid Y	15, mm		
Centroid Z	2,5 mm	-10, mm	15, mm
Moment of Inertia Ip1	2,5568 kg·mm²	7,3516 kg·mm²	
Moment of Inertia Ip2	64,269 kg·mm²	3,6618 kg·mm²	
Moment of Inertia Ip3	66,687 kg·mm²	7,3516 kg·mm²	
Statistics			
Nodes	10815	9108	
Elements	8160	8295	
Mesh Metric	None		

TABLE 4
Model (A4) > Construction Geometry

Object Name	*Construction Geometry*
State	Fully Defined
Display	
Show Mesh	No

TABLE 5
Model (A4) > Construction Geometry > Paths

Object Name	*Path*	*Path 2*
State	Fully Defined	
Definition		
Path Type	Edge	Two Points
Suppressed	No	
Path Coordinate System		Global Coordinate System
Number of Sampling Points		47,
Scope		
Scoping Method	Geometry Selection	
Geometry	1 Edge	
Start		
Coordinate System		Global Coordinate System
Start X Coordinate		0, mm
Start Y Coordinate		0, mm
Start Z Coordinate		12, mm
Location		Defined
End		

Coordinate System		Global Coordinate System
End X Coordinate		0, mm
End Y Coordinate		0, mm
End Z Coordinate		0, mm
Location		Defined

Coordinate Systems

TABLE 6
Model (A4) > Coordinate Systems > Coordinate System

Object Name	*Global Coordinate System*
State	Fully Defined
Definition	
Type	Cartesian
Coordinate System ID	0,
Origin	
Origin X	0, mm
Origin Y	0, mm
Origin Z	0, mm
Directional Vectors	
X Axis Data	[1, 0, 0,]
Y Axis Data	[0, 1, 0,]
Z Axis Data	[0, 0, 1,]

Symmetry

TABLE 7
Model (A4) > Symmetry

Object Name	*Symmetry*
State	Fully Defined

TABLE 8
Model (A4) > Symmetry > Symmetry Region

Object Name	*Symmetry Region*	*Symmetry Region 2*
State	Fully Defined	
Scope		
Scoping Method	Geometry Selection	
Geometry	1 Face	3 Faces
Definition		
Scope Mode	Manual	
Type	Symmetric	
Coordinate System	Global Coordinate System	
Symmetry Normal	X Axis	Y Axis
Suppressed	No	

Connections

TABLE 9
Model (A4) > Connections

Object Name	*Connections*
State	Fully Defined
Auto Detection	

Generate Automatic Connection On Refresh	Yes
Transparency	
Enabled	Yes

TABLE 10
Model (A4) > Connections > Contacts

Object Name	*Contacts*
State	Fully Defined
Definition	
Connection Type	Contact
Scope	
Scoping Method	Geometry Selection
Geometry	All Bodies
Auto Detection	
Tolerance Type	Slider
Tolerance Slider	0,
Tolerance Value	0,40428 mm
Use Range	No
Face/Face	Yes
Cylindrical Faces	Include
Face/Edge	No
Edge/Edge	No
Priority	Include All
Group By	Bodies
Search Across	Bodies
Statistics	
Connections	2
Active Connections	2

TABLE 11
Model (A4) > Connections > Contacts > Contact Regions

Object Name	*Contact Region 3*	*Contact Region 2*
State	Fully Defined	
Scope		
Scoping Method	Geometry Selection	
Contact	2 Faces	1 Face
Target	1 Face	
Contact Bodies	CFRP	
Target Bodies	Solid	
Definition		
Type	Bonded	
Scope Mode	Automatic	
Behavior	Program Controlled	
Trim Contact	Program Controlled	
Trim Tolerance	0,40428 mm	
Suppressed	No	
Advanced		
Formulation	Program Controlled	
Detection Method	Program Controlled	
Penetration Tolerance	Program Controlled	
Elastic Slip Tolerance	Program Controlled	
Normal Stiffness	Program Controlled	
Update Stiffness	Program Controlled	

Pinball Region	Program Controlled
Geometric Modification	
Contact Geometry Correction	None
Target Geometry Correction	None

Mesh

TABLE 12
Model (A4) > Mesh

Object Name	*Mesh*
State	Solved
Display	
Display Style	Body Color
Defaults	
Physics Preference	Mechanical
Relevance	-95
Element Midside Nodes	Dropped
Sizing	
Size Function	Adaptive
Relevance Center	Fine
Element Size	1,50 mm
Initial Size Seed	Active Assembly
Transition	Fast
Span Angle Center	Coarse
Automatic Mesh Based Defeaturing	On
Defeature Size	Default
Minimum Edge Length	5,0 mm
Quality	
Check Mesh Quality	Yes, Errors
Error Limits	Standard Mechanical
Target Quality	Default (0.050000)
Smoothing	Medium
Mesh Metric	None
Inflation	
Use Automatic Inflation	None
Inflation Option	Smooth Transition
Transition Ratio	0,272
Maximum Layers	5
Growth Rate	1,2
Inflation Algorithm	Pre
View Advanced Options	No
Advanced	
Number of CPUs for Parallel Part Meshing	Program Controlled
Straight Sided Elements	
Number of Retries	0
Rigid Body Behavior	Dimensionally Reduced
Mesh Morphing	Disabled
Triangle Surface Mesher	Program Controlled
Topology Checking	No
Pinch Tolerance	Please Define
Generate Pinch on Refresh	No
Statistics	

Nodes	29031
Elements	24750

Static Structural (A5)

TABLE 13
Model (A4) > Analysis

Object Name	*Static Structural (A5)*
State	Solved
Definition	
Physics Type	Structural
Analysis Type	Static Structural
Solver Target	Mechanical APDL
Options	
Environment Temperature	22, °C
Generate Input Only	No

TABLE 14
Model (A4) > Static Structural (A5) > Analysis Settings

Object Name	*Analysis Settings*
State	Fully Defined
Step Controls	
Number Of Steps	1,
Current Step Number	1,
Step End Time	2, s
Auto Time Stepping	Program Controlled
Solver Controls	
Solver Type	Program Controlled
Weak Springs	Off
Solver Pivot Checking	Program Controlled
Large Deflection	Off
Inertia Relief	Off
Rotordynamics Controls	
Coriolis Effect	Off
Restart Controls	
Generate Restart Points	Program Controlled
Retain Files After Full Solve	No
Combined Restart Files	Program Controlled
Nonlinear Controls	
Newton-Raphson Option	Program Controlled
Force Convergence	Program Controlled
Moment Convergence	Program Controlled
Displacement Convergence	Program Controlled
Rotation Convergence	Program Controlled
Line Search	Program Controlled
Stabilization	Off
Output Controls	
Stress	Yes
Strain	Yes
Nodal Forces	No

Contact Miscellaneous	No
General Miscellaneous	No
Store Results At	All Time Points
Analysis Data Management	
Solver Files Directory	C:\ANSYS local files\Cathrine\Bending\CFRP Four point bending test_files\dp0 \SYS\MECH\
Future Analysis	None
Scratch Solver Files Directory	
Save MAPDL db	No
Delete Unneeded Files	Yes
Nonlinear Solution	No
Solver Units	Active System
Solver Unit System	nmm

TABLE 15
Model (A4) > Static Structural (A5) > Loads

Object Name	*Displacement*	*Cylindrical Support*
State	Fully Defined	
Scope		
Scoping Method	Geometry Selection	
Geometry	3 Faces	1 Face
Definition		
Type	Displacement	Cylindrical Support
Define By	Components	
Coordinate System	Global Coordinate System	
X Component	0, mm (ramped)	
Y Component	0, mm (ramped)	
Z Component	-0,3475 mm (ramped)	
Suppressed	No	
Radial		Fixed
Axial		Fixed
Tangential		Fixed

FIGURE 1
Model (A4) > Static Structural (A5) > Displacement

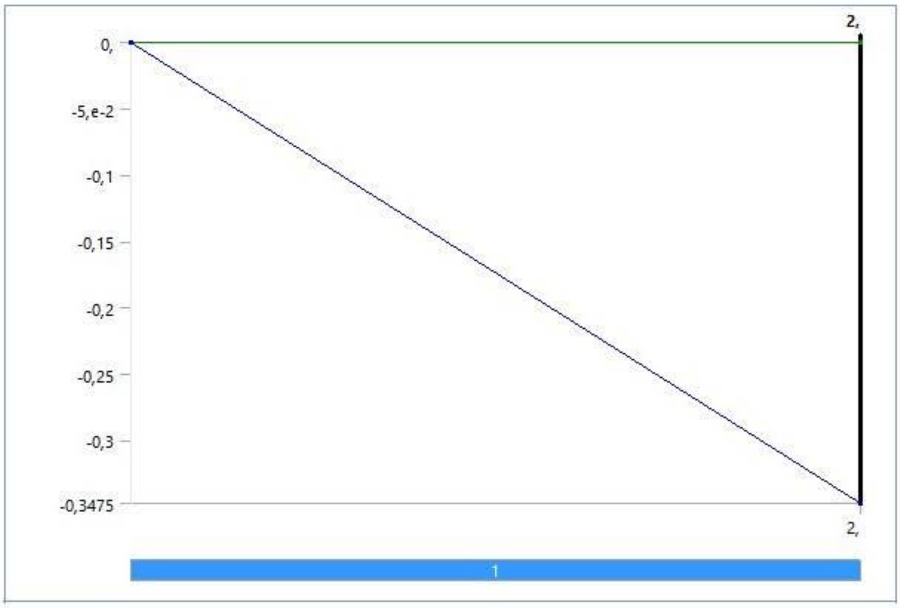

Solution (A6)

TABLE 16
Model (A4) > Static Structural (A5) > Solution

Object Name	*Solution (A6)*
State	Solved
Adaptive Mesh Refinement	
Max Refinement Loops	1,
Refinement Depth	2,
Information	
Status	Done
MAPDL Elapsed Time	5, s
MAPDL Memory Used	208, MB
MAPDL Result File Size	19,75 MB
Post Processing	
Beam Section Results	No

TABLE 17
Model (A4) > Static Structural (A5) > Solution (A6) > Solution Information

Object Name	*Solution Information*
State	Solved
Solution Information	
Solution Output	Solver Output
Newton-Raphson Residuals	0
Identify Element Violations	0
Update Interval	2,5 s
Display Points	All
FE Connection Visibility	

Activate Visibility	Yes
Display	All FE Connectors
Draw Connections Attached To	All Nodes
Line Color	Connection Type
Visible on Results	No
Line Thickness	Single
Display Type	Lines

TABLE 18
Model (A4) > Static Structural (A5) > Solution (A6) > Results

Object Name	*Total Deformation*	*Directional Deformation Z axis*	*Directional Deformation CFRP sample Z axis*
State	Solved		
Scope			
Scoping Method	Geometry Selection		
Geometry	All Bodies		1 Body
Definition			
Type	Total Deformation	Directional Deformation	
By	Time		
Display Time	Last		
Calculate Time History	Yes		
Identifier			
Suppressed	No		
Orientation		Z Axis	
Coordinate System		Global Coordinate System	
Results			
Minimum	0, mm	-0,51442 mm	
Maximum	0,51442 mm	0,24544 mm	
Minimum Occurs On	Solid	CFRP	
Maximum Occurs On	CFRP		
Information			
Time	2, s		
Load Step	1		
Substep	1		
Iteration Number	1		

FIGURE 2
Model (A4) > Static Structural (A5) > Solution (A6) > Total Deformation

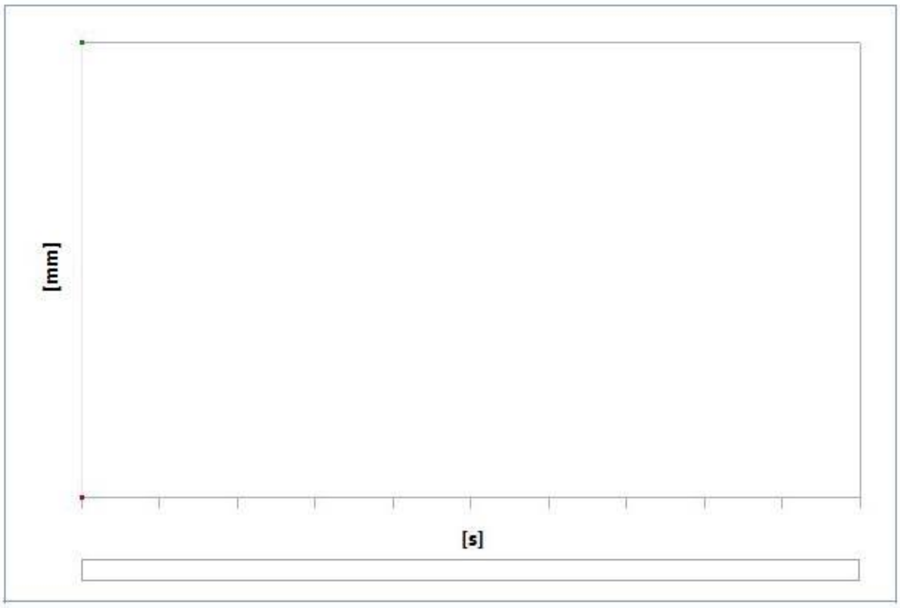

TABLE 19
Model (A4) > Static Structural (A5) > Solution (A6) > Total Deformation

Time [s]	Minimum [mm]	Maximum [mm]
2,	0,	0,51442

FIGURE 3
Model (A4) > Static Structural (A5) > Solution (A6) > Directional Deformation Z axis

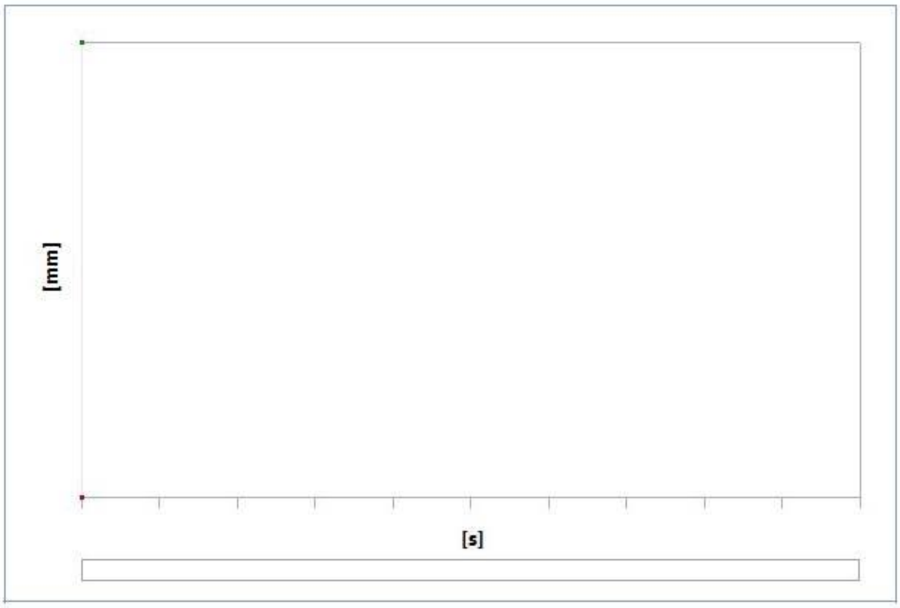

TABLE 20
Model (A4) > Static Structural (A5) > Solution (A6) > Directional Deformation Z axis

Time [s]	Minimum [mm]	Maximum [mm]
2,	-0,51442	0,24544

FIGURE 4
Model (A4) > Static Structural (A5) > Solution (A6) > Directional Deformation CFRP sample Z axis

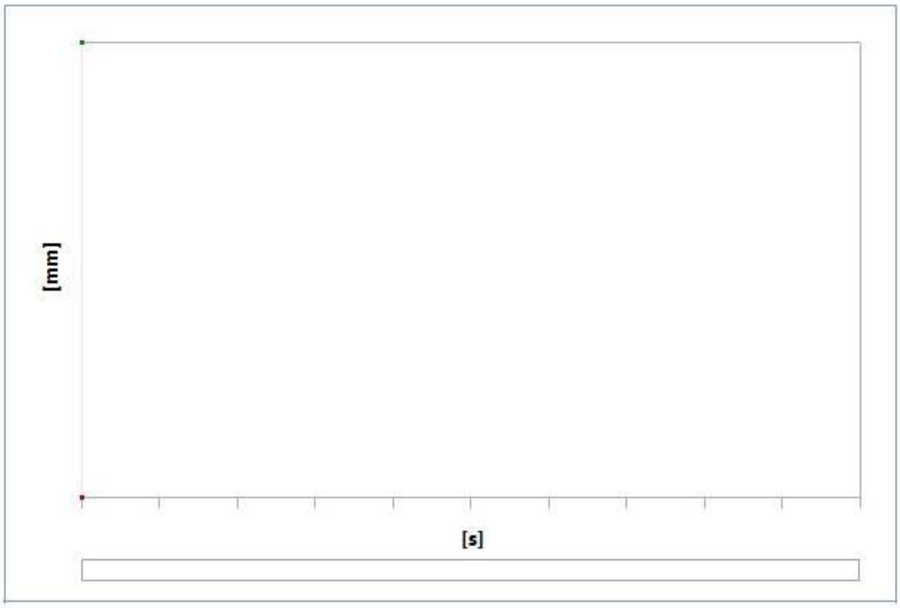

TABLE 21
Model (A4) > Static Structural (A5) > Solution (A6) > Directional Deformation CFRP sample Z axis

Time [s]	Minimum [mm]	Maximum [mm]
2,	-0,51442	0,24544

TABLE 22
Model (A4) > Static Structural (A5) > Solution (A6) > Probes

Object Name	*Force Reaction*
State	Solved
Definition	
Type	Force Reaction
Location Method	Boundary Condition
Boundary Condition	Displacement
Orientation	Global Coordinate System
Suppressed	No
Options	
Result Selection	All
Display Time	2, s
Results	
X Axis	7066,8 N
Y Axis	95,552 N
Z Axis	142,42 N
Total	7068,9 N
Maximum Value Over Time	
X Axis	7066,8 N
Y Axis	95,552 N
Z Axis	142,42 N
Total	7068,9 N

Minimum Value Over Time	
X Axis	7066,8 N
Y Axis	95,552 N
Z Axis	142,42 N
Total	7068,9 N
Information	
Time	2, s
Load Step	1
Substep	1
Iteration Number	1

FIGURE 5
Model (A4) > Static Structural (A5) > Solution (A6) > Force Reaction

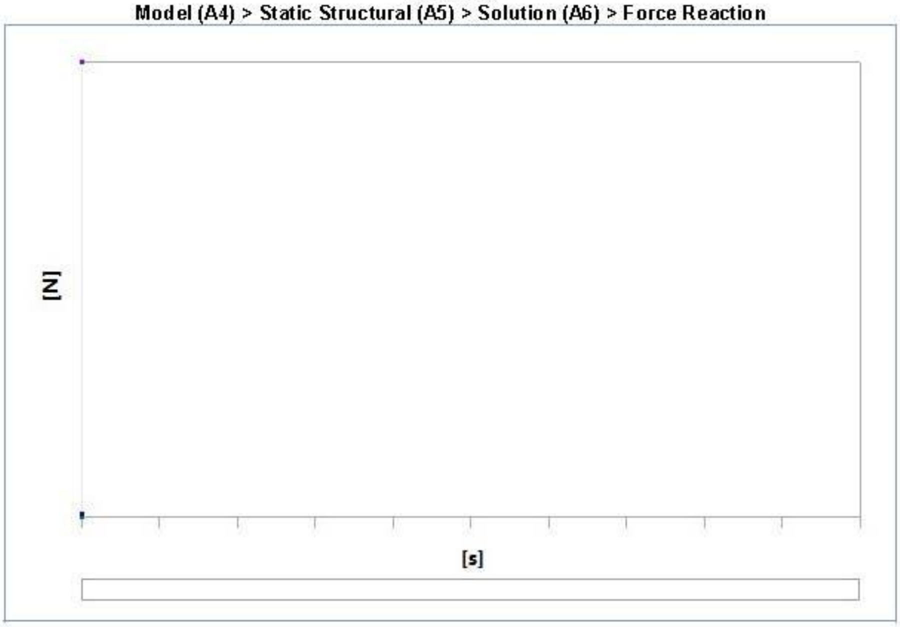

TABLE 23
Model (A4) > Static Structural (A5) > Solution (A6) > Force Reaction

Time [s]	Force Reaction (X) [N]	Force Reaction (Y) [N]	Force Reaction (Z) [N]	Force Reaction (Total) [N]
2,	7066,8	95,552	142,42	7068,9

Material Data

Epoxy Carbon Woven (230 GPa) Wet

TABLE 24
Epoxy Carbon Woven (230 GPa) Wet > Constants

Density	1,451e-006 kg mm^-3

TABLE 25
Epoxy Carbon Woven (230 GPa) Wet > Orthotropic Elasticity

Young's Modulus X direction MPa	Young's Modulus Y direction MPa	Young's Modulus Z direction MPa	Poisson's Ratio XY	Poisson's Ratio YZ	Poisson's Ratio XZ	Shear Modulus XY MPa	Shear Modulus YZ MPa	Shear Modulus XZ MPa
59160	59160	7500,	4,e-002	0,3	0,3	17500	2700,	2700,

TABLE 26
Epoxy Carbon Woven (230 GPa) Wet > Orthotropic Strain Limits

Tensile X direction	Tensile Y direction	Tensile Z direction	Compressive X direction	Compressive Y direction	Compressive Z direction	Shear XY	Shear YZ	Shear XZ
9,2e-003	9,2e-003	7,8e-003	-8,4e-003	-8,4e-003	-1,1e-002	2,e-002	1,5e-002	1,5e-002

TABLE 27
Epoxy Carbon Woven (230 GPa) Wet > Orthotropic Stress Limits

Tensile X direction MPa	Tensile Y direction MPa	Tensile Z direction MPa	Compressive X direction MPa	Compressive Y direction MPa	Compressive Z direction MPa	Shear XY MPa	Shear YZ MPa	Shear XZ MPa
513,	513,	50,	-437,	-437,	-150,	120,	55,	55,

TABLE 28
Epoxy Carbon Woven (230 GPa) Wet > Orthotropic Secant Coefficient of Thermal Expansion

Temperature C	Coefficient of Thermal Expansion X direction C^-1	Coefficient of Thermal Expansion Y direction C^-1	Coefficient of Thermal Expansion Z direction C^-1
	2,2e-006	2,2e-006	1,e-005

Zero-Thermal-Strain Reference Temperature C
20,

TABLE 29
Epoxy Carbon Woven (230 GPa) Wet > Tsai-Wu Constants

Temperature C	Coupling Coefficient XY	Coupling Coefficient YZ	Coupling Coefficient XZ
	-1,	-1,	-1,

TABLE 30
Epoxy Carbon Woven (230 GPa) Wet > Color

Red	Green	Blue
170,	170,	170,

Structural Steel

TABLE 31
Structural Steel > Constants

Density	7,85e-006 kg mm^-3
Coefficient of Thermal Expansion	1,2e-005 C^-1
Specific Heat	4,34e+005 mJ kg^-1 C^-1
Thermal Conductivity	6,05e-002 W mm^-1 C^-1
Resistivity	1,7e-004 ohm mm

TABLE 32
Structural Steel > Color

Red	Green	Blue
132,	139,	179,

TABLE 33
Structural Steel > Compressive Ultimate Strength

Compressive Ultimate Strength MPa
0,

TABLE 34
Structural Steel > Compressive Yield Strength

Compressive Yield Strength MPa
250,

TABLE 35
Structural Steel > Tensile Yield Strength

Tensile Yield Strength MPa
250,

TABLE 36
Structural Steel > Tensile Ultimate Strength

Tensile Ultimate Strength MPa
460,

TABLE 37
Structural Steel > Isotropic Secant Coefficient of Thermal Expansion

Zero-Thermal-Strain Reference Temperature C
22,

TABLE 38
Structural Steel > Alternating Stress Mean Stress

Alternating Stress MPa	Cycles	Mean Stress MPa
3999,	10,	0,
2827,	20,	0,
1896,	50,	0,
1413,	100,	0,
1069,	200,	0,
441,	2000,	0,
262,	10000	0,
214,	20000	0,
138,	1,e+005	0,
114,	2,e+005	0,
86,2	1,e+006	0,

TABLE 39
Structural Steel > Strain-Life Parameters

Strength Coefficient MPa	Strength Exponent	Ductility Coefficient	Ductility Exponent	Cyclic Strength Coefficient MPa	Cyclic Strain Hardening Exponent
920,	-0,106	0,213	-0,47	1000,	0,2

TABLE 40
Structural Steel > Isotropic Elasticity

Temperature C	Young's Modulus MPa	Poisson's Ratio	Bulk Modulus MPa	Shear Modulus MPa
	2,e+005	0,3	1,6667e+005	76923

TABLE 41
Structural Steel > Isotropic Relative Permeability

Relative Permeability

10000

Appendix B – ANSYS Workbench data of the air gun impact test

Project

First Saved	Monday, March 13, 2017
Last Saved	Tuesday, May 16, 2017
Product Version	18.0 Release
Save Project Before Solution	No
Save Project After Solution	No

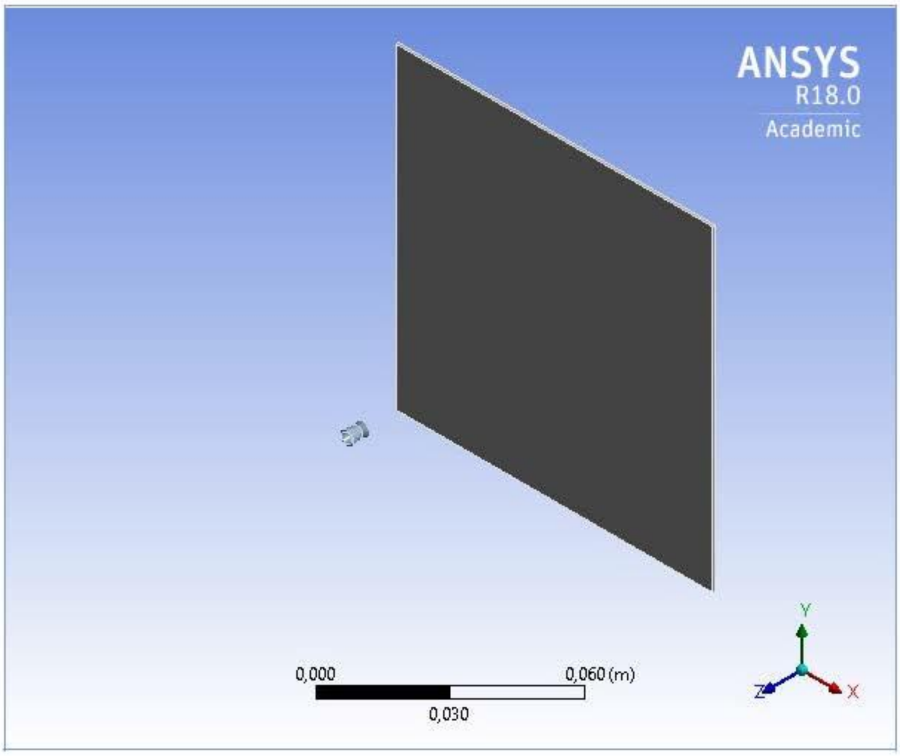

Contents

Report Not Finalized

Not all objects described below are in a finalized state. As a result, data may be incomplete, obsolete or in error. View first state problem. To finalize this report, edit objects as needed and solve the analyses.

Units

TABLE 1

Unit System	Metric (m, kg, N, s, V, A) Degrees rad/s Celsius
Angle	Degrees
Rotational Velocity	rad/s
Temperature	Celsius

Model (A4)

Geometry

TABLE 2
Model (A4) > Geometry

Object Name	*Geometry*
State	Fully Defined
Definition	
Source	C:\ANSYS local files\Cathrine\Room temperature\Air gun impact single layer_files\dp0\SYS\DM\SYS.agdb

Type	DesignModeler
Length Unit	Meters
Display Style	Body Color
Bounding Box	
Length X	0,1 m
Length Y	0,1 m
Length Z	6,6294e-002 m
Properties	
Volume	7,9757e-006 m³
Mass	1,195e-002 kg
Scale Factor Value	1,
Statistics	
Bodies	2
Active Bodies	2
Nodes	9193
Elements	13786
Mesh Metric	None
Basic Geometry Options	
Parameters	Independent
Parameter Key	
Attributes	Yes
Attribute Key	
Named Selections	Yes
Named Selection Key	
Material Properties	Yes
Advanced Geometry Options	
Use Associativity	Yes
Coordinate Systems	Yes
Coordinate System Key	
Reader Mode Saves Updated File	No
Use Instances	Yes
Smart CAD Update	Yes
Compare Parts On Update	No
Attach File Via Temp File	Yes
Temporary Directory	C:\Users\cst037\AppData\Roaming\Ansys\v172
Analysis Type	3-D
Decompose Disjoint Geometry	Yes
Enclosure and Symmetry Processing	Yes

TABLE 3
Model (A4) > Geometry > Parts

Object Name	*CFRP sample*	*Pellet*
State	Meshed	
Graphics Properties		
Visible	Yes	
Transparency	1	
Definition		
Suppressed	No	
Stiffness Behavior	Flexible	
Coordinate System	Default Coordinate System	

Reference Temperature	By Environment	
Reference Frame	Lagrangian	
Material		
Assignment	Epoxy Carbon Woven (230 GPa) Wet	Lead
Bounding Box		
Length X	0,1 m	4,4e-003 m
Length Y	0,1 m	4,4e-003 m
Length Z	7,9375e-004 m	5,5e-003 m
Properties		
Volume	7,9375e-006 m³	3,8153e-008 m³
Mass	1,1517e-002 kg	4,325e-004 kg
Centroid X	5,e-002 m	5,0007e-002 m
Centroid Y	5,e-002 m	
Centroid Z	-3,9687e-004 m	6,251e-002 m
Moment of Inertia Ip1	9,5984e-006 kg·m²	1,8418e-009 kg·m²
Moment of Inertia Ip2	9,5984e-006 kg·m²	1,8416e-009 kg·m²
Moment of Inertia Ip3	1,9196e-005 kg·m²	1,0957e-009 kg·m²
Statistics		
Nodes	6962	2231
Elements	3364	10422
Mesh Metric	None	

Coordinate Systems

TABLE 4
Model (A4) > Coordinate Systems > Coordinate System

Object Name	*Global Coordinate System*
State	Fully Defined
Definition	
Type	Cartesian
Origin	
Origin X	0, m
Origin Y	0, m
Origin Z	0, m
Directional Vectors	
X Axis Data	[1, 0, 0,]
Y Axis Data	[0, 1, 0,]
Z Axis Data	[0, 0, 1,]

Connections

TABLE 5
Model (A4) > Connections

Object Name	*Connections*
State	Fully Defined
Auto Detection	
Generate Automatic Connection On Refresh	Yes
Transparency	
Enabled	Yes

TABLE 6
Model (A4) > Connections > Body Interactions

Object Name	*Body Interactions*
State	Fully Defined
Advanced	
Contact Detection	Trajectory
Formulation	Penalty
Sliding Contact	Discrete Surface
Body Self Contact	Program Controlled
Element Self Contact	Program Controlled
Tolerance	0,2

TABLE 7
Model (A4) > Connections > Body Interactions > Body Interaction

Object Name	*Body Interaction*
State	Fully Defined
Scope	
Scoping Method	Geometry Selection
Geometry	All Bodies
Definition	
Type	Frictionless
Suppressed	No

Mesh

TABLE 8
Model (A4) > Mesh

Object Name	*Mesh*
State	Solved
Display	
Display Style	Body Color
Defaults	
Physics Preference	Explicit
Relevance	70
Element Midside Nodes	Dropped
Sizing	
Size Function	Adaptive
Relevance Center	Fine
Element Size	Default
Initial Size Seed	Active Assembly
Transition	Slow
Span Angle Center	Fine
Automatic Mesh Based Defeaturing	On
Defeature Size	Default
Minimum Edge Length	7,9375e-004 m
Quality	
Check Mesh Quality	Yes, Errors
Target Quality	Default (0.050000)
Smoothing	High
Mesh Metric	None
Inflation	
Use Automatic Inflation	None
Inflation Option	Smooth Transition
Transition Ratio	0,272

Maximum Layers	5
Growth Rate	1,2
Inflation Algorithm	Pre
View Advanced Options	No
Advanced	
Number of CPUs for Parallel Part Meshing	Program Controlled
Straight Sided Elements	
Number of Retries	0
Rigid Body Behavior	Full Mesh
Mesh Morphing	Disabled
Triangle Surface Mesher	Program Controlled
Topology Checking	No
Pinch Tolerance	Please Define
Generate Pinch on Refresh	No
Statistics	
Nodes	9193
Elements	13786

Explicit Dynamics (A5)

TABLE 9
Model (A4) > Analysis

Object Name	*Explicit Dynamics (A5)*
State	Solved
Definition	
Physics Type	Structural
Analysis Type	Explicit Dynamics
Solver Target	AUTODYN
Options	
Environment Temperature	22, °C
Generate Input Only	No

TABLE 10
Model (A4) > Explicit Dynamics (A5) > Initial Conditions

Object Name	*Initial Conditions*
State	Fully Defined

TABLE 11
Model (A4) > Explicit Dynamics (A5) > Initial Conditions > Initial Condition

Object Name	*Pre-Stress (None)*	*Velocity*
State	Fully Defined	
Definition		
Pre-Stress Environment	None	
Pressure Initialization	From Deformed State	
Input Type		Velocity
Define By		Components
Coordinate System		Global Coordinate System
X Component		0, m/s
Y Component		0, m/s
Z Component		-160, m/s
Suppressed		No
Scope		

Scoping Method	Geometry Selection
Geometry	1 Body

TABLE 12
Model (A4) > Explicit Dynamics (A5) > Analysis Settings

Object Name	*Analysis Settings*
State	Fully Defined
Analysis Settings Preference	
Type	Program Controlled
Step Controls	
Resume From Cycle	0
Maximum Number of Cycles	1e+07
End Time	7,e-004 s
Maximum Energy Error	0,1
Reference Energy Cycle	0
Initial Time Step	Program Controlled
Minimum Time Step	Program Controlled
Maximum Time Step	Program Controlled
Time Step Safety Factor	0,9
Characteristic Dimension	Diagonals
Automatic Mass Scaling	No
Solver Controls	
Solve Units	mm, mg, ms
Beam Solution Type	Bending
Beam Time Step Safety Factor	0,5
Hex Integration Type	Exact
Shell Sublayers	3
Shell Shear Correction Factor	0,8333
Shell BWC Warp Correction	Yes
Shell Thickness Update	Nodal
Tet Integration	Average Nodal Pressure
Shell Inertia Update	Recompute
Density Update	Program Controlled
Minimum Velocity	1,e-006 m s^-1
Maximum Velocity	1,e+010 m s^-1
Radius Cutoff	1,e-003
Minimum Strain Rate Cutoff	1,e-010
Euler Domain Controls	
Domain Size Definition	Program Controlled
Display Euler Domain	Yes
Scope	All Bodies
X Scale factor	1,2
Y Scale factor	1,2
Z Scale factor	1,2
Domain Resolution Definition	Total Cells
Total Cells	2,5e+05
Lower X Face	Flow Out
Lower Y Face	Flow Out
Lower Z Face	Flow Out
Upper X Face	Flow Out

Upper Y Face	Flow Out
Upper Z Face	Flow Out
Euler Tracking	By Body
Damping Controls	
Linear Artificial Viscosity	0,2
Quadratic Artificial Viscosity	1,
Linear Viscosity in Expansion	No
Artificial Viscosity For Shells	Yes
Hourglass Damping	AUTODYN Standard
Viscous Coefficient	0,1
Static Damping	0,
Erosion Controls	
On Geometric Strain Limit	Yes
Geometric Strain Limit	1,5
On Material Failure	No
On Minimum Element Time Step	No
Retain Inertia of Eroded Material	Yes
Output Controls	
Save Results on	Equally Spaced Points
Result Number Of Points	20
Save Restart Files on	Equally Spaced Points
Restart Number Of Points	5
Save Result Tracker Data on	Cycles
Tracker Cycles	1
Output Contact Forces	Off
Analysis Data Management	
Solver Files Directory	C:\ANSYS local files\Cathrine\Room temperature\Air gun impact single layer_files\dp0\SYS\MECH\
Scratch Solver Files Directory	

TABLE 13
Model (A4) > Explicit Dynamics (A5) > Loads

Object Name	*Fixed Support*
State	Fully Defined
Scope	
Scoping Method	Geometry Selection
Geometry	4 Faces
Definition	
Type	Fixed Support
Suppressed	No

Solution (A6)

TABLE 14
Model (A4) > Explicit Dynamics (A5) > Solution

Object Name	*Solution (A6)*
State	Solved
Information	

Status	Done
Post Processing	
Beam Section Results	No

TABLE 15
Model (A4) > Explicit Dynamics (A5) > Solution (A6) > Solution Information

Object Name	*Solution Information*
State	Solved
Solution Information	
Solution Output	Solver Output
Update Interval	2,5 s
Display Points	All
Display Filter During Solve	Yes

TABLE 16
Model (A4) > Explicit Dynamics (A5) > Solution (A6) > Results

Object Name	*Total Deformation*	*Shear Elastic Strain*	*Equivalent Stress*
State	Solved		
Scope			
Scoping Method	Geometry Selection		
Geometry	All Bodies		
Definition			
Type	Total Deformation	Shear Elastic Strain	Equivalent (von-Mises) Stress
By	Time		
Display Time	2,5128e-005 s	Last	
Calculate Time History	Yes		
Identifier			
Suppressed	No		
Orientation		XY Plane	
Coordinate System		Global Coordinate System	
Results			
Minimum	0, m	-0,94595 m/m	4,3457e+005 Pa
Maximum	5,6008e-003 m	8,2178e-002 m/m	2,8592e+008 Pa
Minimum Occurs On	CFRP sample		
Maximum Occurs On	Pellet	CFRP sample	Pellet
Minimum Value Over Time			
Minimum	0, m	-0,94825 m/m	0, Pa
Maximum	0, m	0, m/m	1,695e+006 Pa
Maximum Value Over Time			
Minimum	0, m	0, m/m	0, Pa
Maximum	8,2938e-002 m	0,11473 m/m	5,5117e+008 Pa
Information			
Time	3,5005e-005 s	7,e-004 s	
Set	2	21	
Cycle Number	1631	36391	
Integration Point Results			
Display Option		Averaged	
Average Across Bodies		No	

FIGURE 1
Model (A4) > Explicit Dynamics (A5) > Solution (A6) > Total Deformation

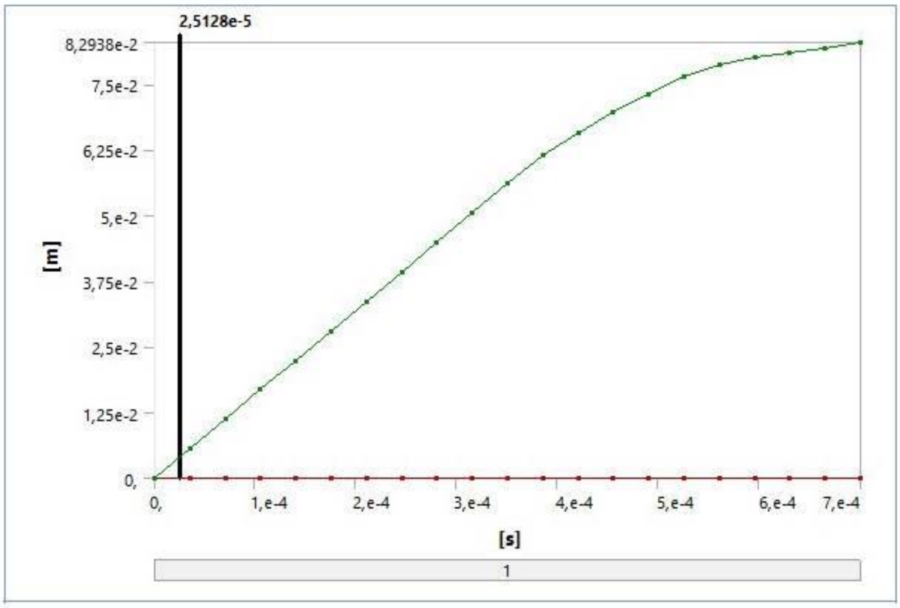

TABLE 17
Model (A4) > Explicit Dynamics (A5) > Solution (A6) > Total Deformation

Time [s]	Minimum [m]	Maximum [m]
1,1755e-038	0,	0,
3,5005e-005		5,6008e-003
7,0005e-005		1,1201e-002
1,05e-004		1,6801e-002
1,4e-004		2,2401e-002
1,75e-004		2,8001e-002
2,1e-004		3,3601e-002
2,45e-004		3,9201e-002
2,8e-004		4,4801e-002
3,15e-004		5,0401e-002
3,5e-004		5,6001e-002
3,8502e-004		6,1443e-002
4,2e-004		6,5747e-002
4,5501e-004		6,9641e-002
4,9002e-004		7,3185e-002
5,2502e-004		7,6333e-002
5,6e-004		7,8754e-002
5,9501e-004		8,0118e-002
6,3001e-004		8,1032e-002
6,65e-004		8,1942e-002
7,e-004		8,2938e-002

FIGURE 2
Model (A4) > Explicit Dynamics (A5) > Solution (A6) > Shear Elastic Strain

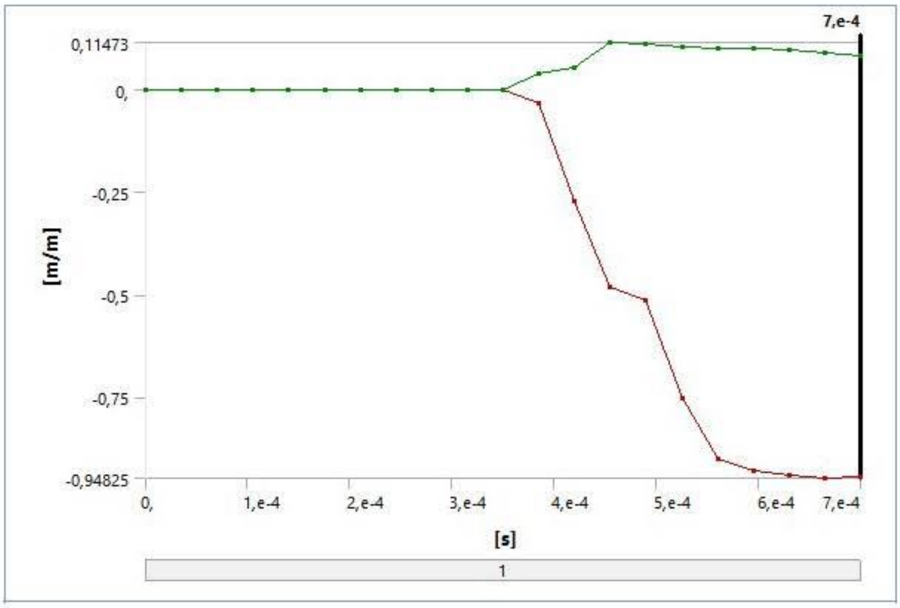

TABLE 18
Model (A4) > Explicit Dynamics (A5) > Solution (A6) > Shear Elastic Strain

Time [s]	Minimum [m/m]	Maximum [m/m]
1,1755e-038	0,	0,
3,5005e-005		
7,0005e-005		
1,05e-004		
1,4e-004		
1,75e-004		
2,1e-004		
2,45e-004		
2,8e-004		
3,15e-004		
3,5e-004		
3,8502e-004	-3,4311e-002	3,7914e-002
4,2e-004	-0,27103	5,3386e-002
4,5501e-004	-0,48163	0,11473
4,9002e-004	-0,5139	0,11214
5,2502e-004	-0,752	0,10452
5,6e-004	-0,89986	9,9966e-002
5,9501e-004	-0,93032	9,8481e-002
6,3001e-004	-0,94268	9,6329e-002
6,65e-004	-0,94825	8,8208e-002
7,e-004	-0,94595	8,2178e-002

FIGURE 3
Model (A4) > Explicit Dynamics (A5) > Solution (A6) > Equivalent Stress

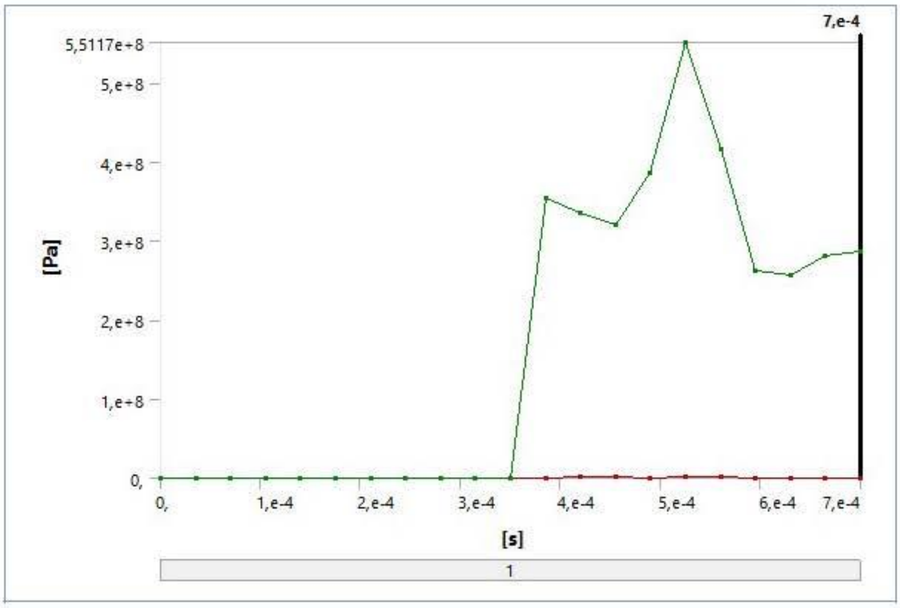

TABLE 19
Model (A4) > Explicit Dynamics (A5) > Solution (A6) > Equivalent Stress

Time [s]	Minimum [Pa]	Maximum [Pa]
1,1755e-038	0,	0,
3,5005e-005		
7,0005e-005		
1,05e-004		
1,4e-004		
1,75e-004		
2,1e-004		
2,45e-004		
2,8e-004		
3,15e-004		
3,5e-004		
3,8502e-004	37272	3,5431e+008
4,2e-004	1,695e+006	3,3589e+008
4,5501e-004	1,5505e+006	3,2123e+008
4,9002e-004	4,6111e+005	3,8551e+008
5,2502e-004	1,2527e+006	5,5117e+008
5,6e-004	1,3191e+006	4,1534e+008
5,9501e-004	3,0409e+005	2,6175e+008
6,3001e-004	5,9936e+005	2,5751e+008
6,65e-004	4,3328e+005	2,8031e+008
7,e-004	4,3457e+005	2,8592e+008

Material Data

Epoxy Carbon Woven (230 GPa) Wet

TABLE 20
Epoxy Carbon Woven (230 GPa) Wet > Constants

Density	1451, kg m^-3

TABLE 21
Epoxy Carbon Woven (230 GPa) Wet > Orthotropic Elasticity

Young's Modulus X direction Pa	Young's Modulus Y direction Pa	Young's Modulus Z direction Pa	Poisson's Ratio XY	Poisson's Ratio YZ	Poisson's Ratio XZ	Shear Modulus XY Pa	Shear Modulus YZ Pa	Shear Modulus XZ Pa
5,916e+010	5,916e+010	7,5e+009	4,e-002	0,3	0,3	1,75e+010	2,7e+009	2,7e+009

TABLE 22
Epoxy Carbon Woven (230 GPa) Wet > Orthotropic Strain Limits

Tensile X direction	Tensile Y direction	Tensile Z direction	Compressive X direction	Compressive Y direction	Compressive Z direction	Shear XY	Shear YZ	Shear XZ
9,2e-003	9,2e-003	7,8e-003	-8,4e-003	-8,4e-003	-1,1e-002	2,e-002	1,5e-002	1,5e-002

TABLE 23
Epoxy Carbon Woven (230 GPa) Wet > Orthotropic Stress Limits

Tensile X direction Pa	Tensile Y direction Pa	Tensile Z direction Pa	Compressive X direction Pa	Compressive Y direction Pa	Compressive Z direction Pa	Shear XY Pa	Shear YZ Pa	Shear XZ Pa
5,13e+008	5,13e+008	5,e+007	-4,37e+008	-4,37e+008	-1,5e+008	1,2e+008	5,5e+007	5,5e+007

TABLE 24
Epoxy Carbon Woven (230 GPa) Wet > Orthotropic Secant Coefficient of Thermal Expansion

Temperature C	Coefficient of Thermal Expansion X direction C^-1	Coefficient of Thermal Expansion Y direction C^-1	Coefficient of Thermal Expansion Z direction C^-1
	2,2e-006	2,2e-006	1,e-005
Zero-Thermal-Strain Reference Temperature C			
20,			

TABLE 25
Epoxy Carbon Woven (230 GPa) Wet > Tsai-Wu Constants

Temperature C	Coupling Coefficient XY	Coupling Coefficient YZ	Coupling Coefficient XZ
	-1,	-1,	-1,

TABLE 26
Epoxy Carbon Woven (230 GPa) Wet > Color

Red	Green	Blue
103,	192,	205,

Lead

TABLE 27
Lead > Constants

Thermal Conductivity	35, W m^-1 C^-1
Density	11336 kg m^-3

Specific Heat	129, J kg^-1 C^-1

TABLE 28
Lead > Color

Red	Green	Blue
181,	194,	156,

TABLE 29
Lead > Isotropic Elasticity

Temperature C	Young's Modulus Pa	Poisson's Ratio	Bulk Modulus Pa	Shear Modulus Pa
	1,25e+010	0,44	3,4722e+010	4,3403e+009

Appendix C – Speed test of Diabolo pellet

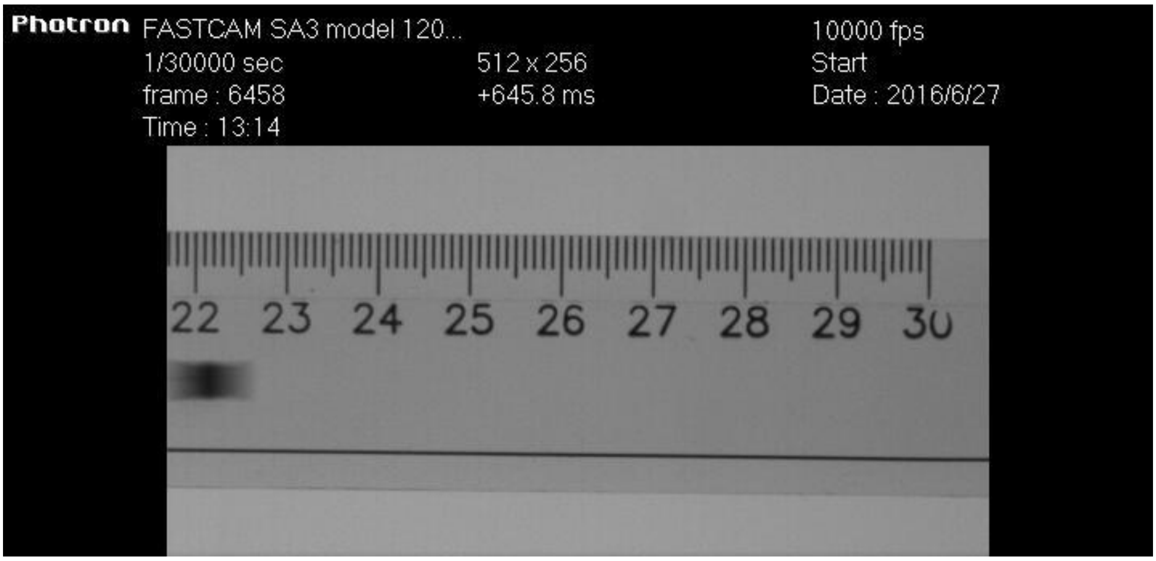

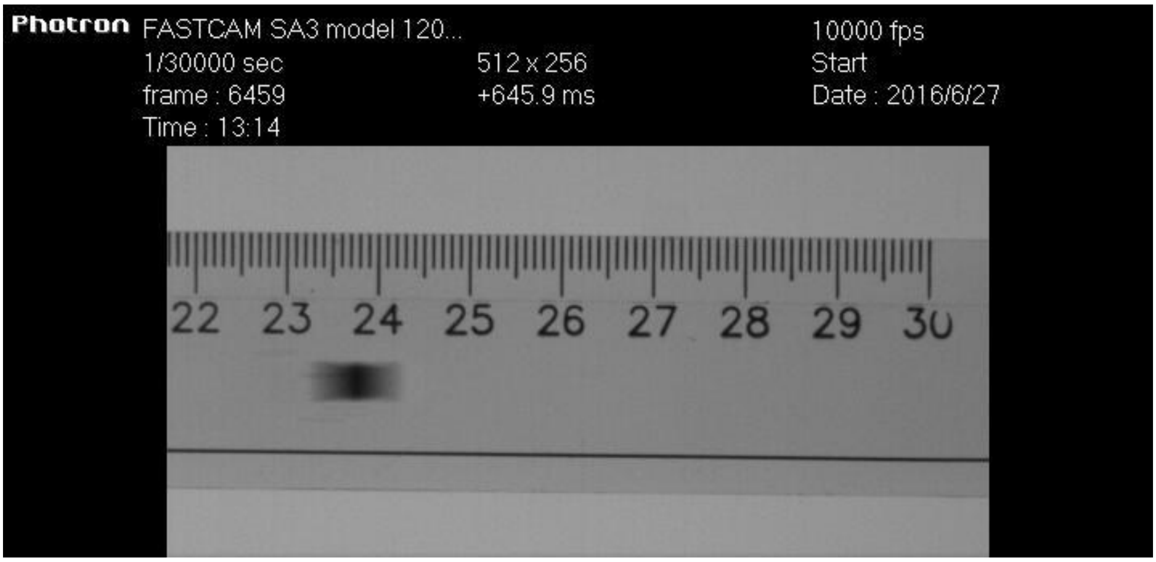

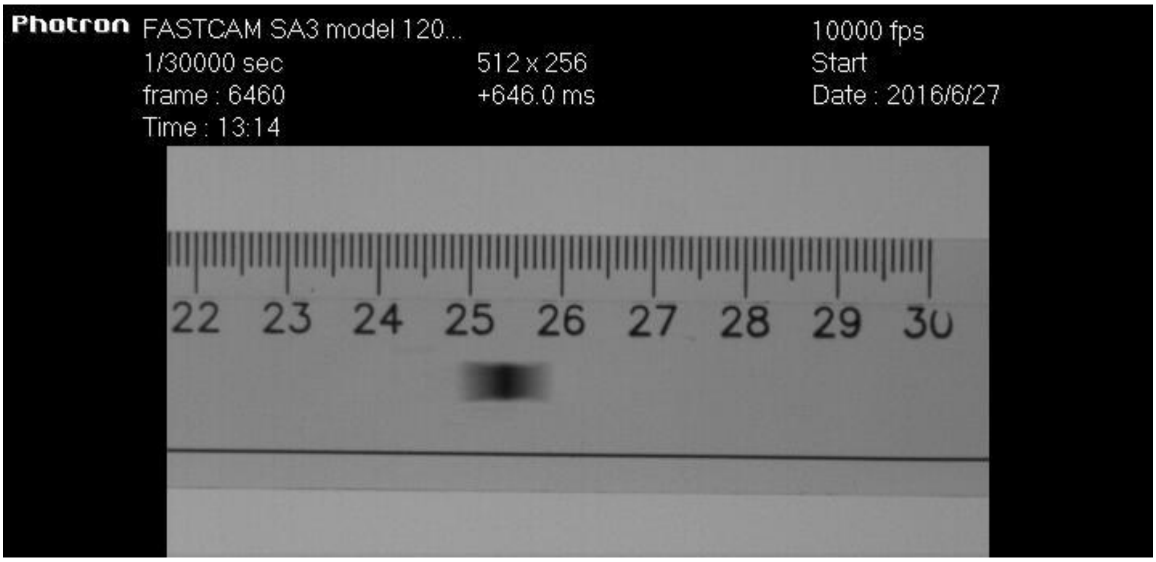

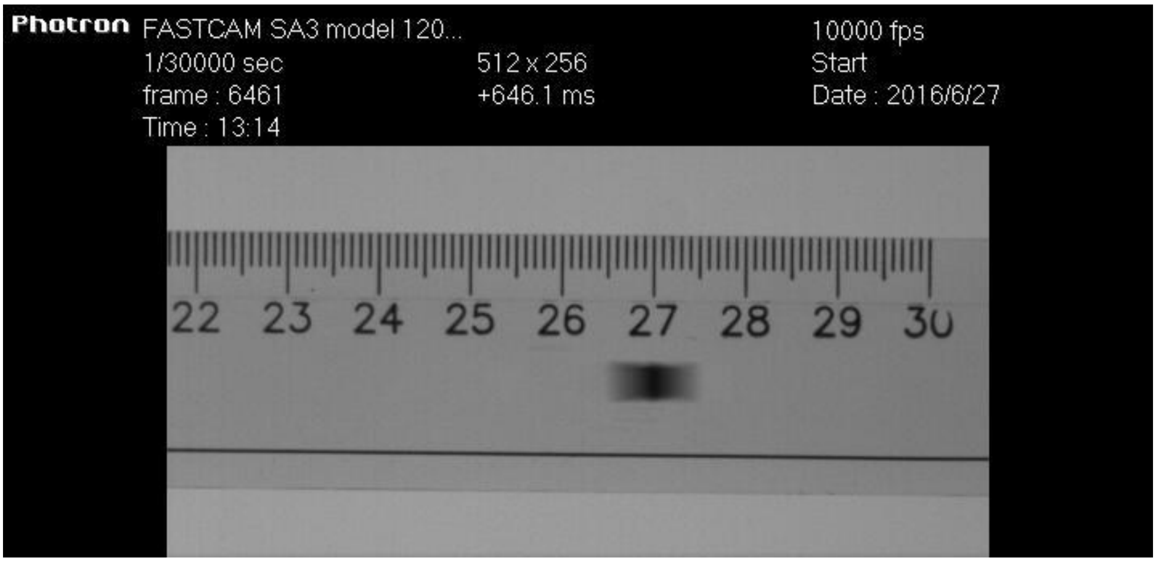
Photron FASTCAM SA3 model 120...
1/30000 sec
frame : 6461
Time : 13:14
512 x 256
+646.1 ms
10000 fps
Start
Date : 2016/6/27
22 23 24 25 26 27 28 29 30

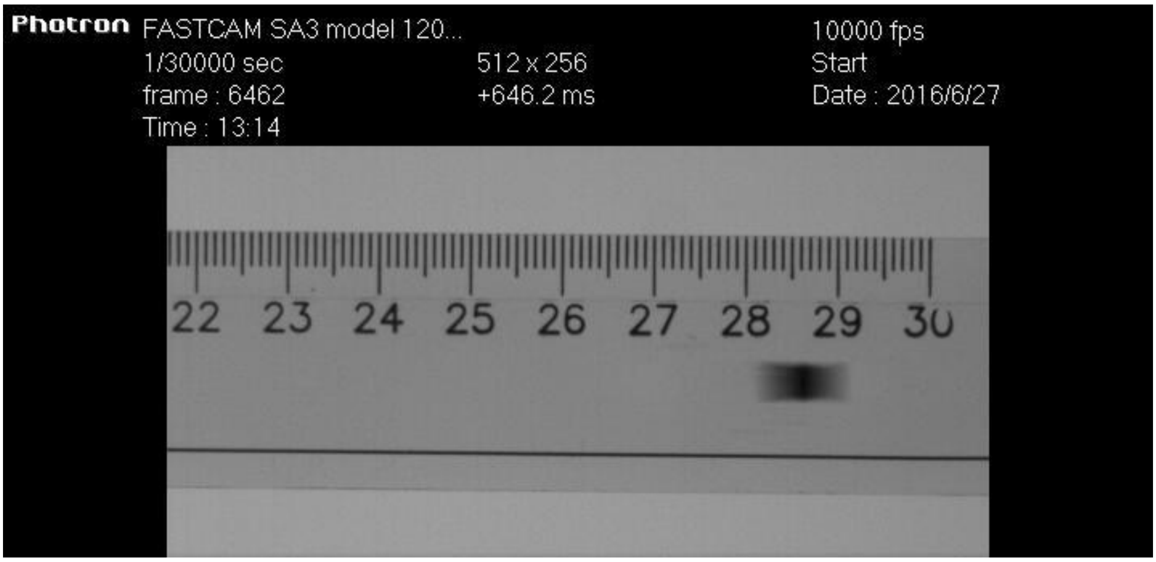
Photron FASTCAM SA3 model 120...
1/30000 sec
frame : 6462
Time : 13:14
512 x 256
+646.2 ms
10000 fps
Start
Date : 2016/6/27
22 23 24 25 26 27 28 29 30

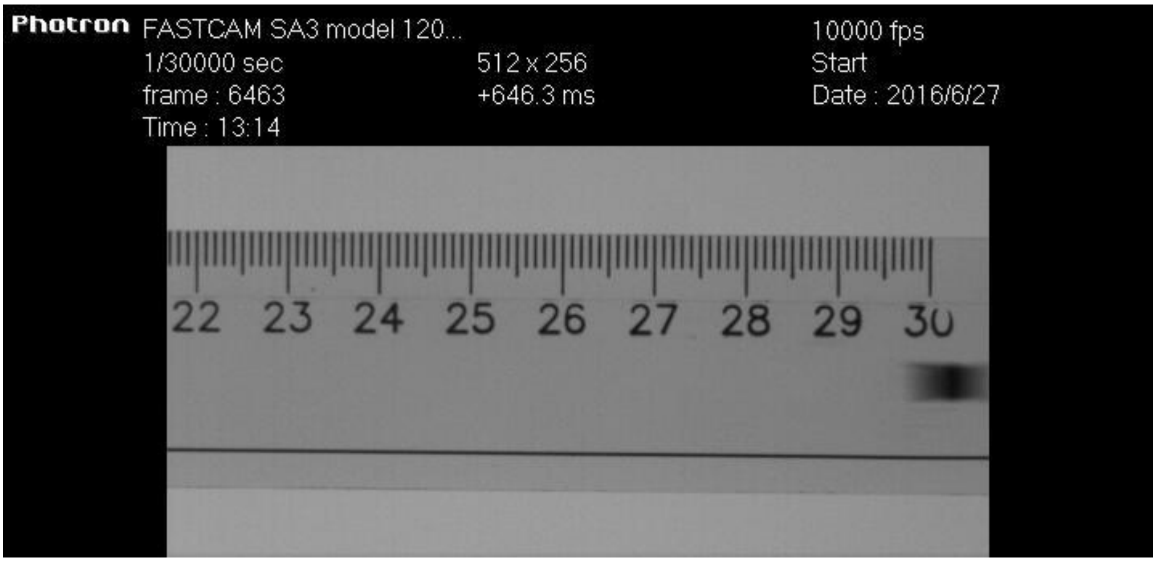
Photron FASTCAM SA3 model 120...
1/30000 sec
frame : 6463
Time : 13:14
512 x 256
+646.3 ms
10000 fps
Start
Date : 2016/6/27
22 23 24 25 26 27 28 29 30

Appendix D – Charpy test results

Quantitative Charpy test results

Reading at cold room (about -20 degrees) (kpm, kilo pound meter)	Nm (Newton meter)	Reading at room temperature (about 22 degrees) (kpm, kilo pound meter)	Nm (Newton meter)	Reading after cyclic temperature changes (kpm, kilo pound meter)	Nm (Newton meter)
0,34	3,3354	0,39	3,8259	0,3	2,943
0,34	3,3354	0,43	4,2183	0,3	2,943
0,36	3,5316	0,44	4,3164	0,33	3,2373
0,4	3,924	0,465	4,56165	0,42	4,1202
0,43	4,2183	0,47	4,6107	0,45	4,4145
0,43	4,2183	0,48	4,7088	0,46	4,5126
0,44	4,3164	0,54	5,2974	0,46	4,5126
0,44	4,3164	0,55	5,3955	0,49	4,8069
0,45	4,4145	0,61	5,9841	0,5	4,905
0,55	5,3955	0,62	6,0822	0,52	5,1012
0,55	5,3955	0,63	6,1803	0,53	5,1993
0,585	5,73885	0,64	6,2784	0,61	5,9841
0,65	6,3765	0,665	6,52365	0,66	6,4746
0,68	6,6708	0,67	6,5727	0,66	6,4746
0,72	7,0632	0,75	7,3575	0,7	6,867
0,77	7,5537	0,77	7,5537	0,71	6,9651
0,78	7,6518	0,84	8,2404	0,86	8,4366
0,82	8,0442	0,85	8,3385	0,87	8,5347
0,99	9,7119	0,89	8,7309	0,99	9,7119
Average	5,305575		5,89145		5,35735

Population standard deviation	1,532916047		1,343974862		1,631772231

Qualitative Charpy test results

	Cut off (Fiber-dominated failure)	Delamination (Matrix-dominated failure)	Total
Number of failures #	13	41	54
Percentage %	24	76	100